NASA TECHNICAL MEMORANDUM

NASA TM X-72745

NASA TM X-72745

THE EFFECT OF WING DIHEDRAL AND SECTION SUCTION DISTRIBUTION ON VORTEX BURSTING

BY

Karen E. Washburn

and

Blair B. Gloss

July 10, 1975

NATIONAL AERONAUTICS AND SPACE ADMINISTRATION

LANGLEY RESEARCH CENTER, HAMPTON, VIRGINIA 23665

1. Report No.	2. Government Accession No.	3. Recipient's Catalog No.
NASA TM X-72745		

4. Title and Subtitle	5. Report Date
The Effect of Wing Dihedral and Section Suction Distribution on Vortex Bursting	AUGUST 1975
	6. Performing Organization Code

7. Author(s)	8. Performing Organization Report No.
Karen E. Washburn and Blair B. Gloss	
	10. Work Unit No. 505-11-21-02

9. Performing Organization Name and Address	11. Contract or Grant No.
NASA Langley Research Center Hampton, VA 23665	
	13. Type of Report and Period Covered
12. Sponsoring Agency Name and Address	Technical Memorandum
National Aeronautics & Space Administration Washington, DC 20546	14. Sponsoring Agency Code

15. Supplementary Notes

Final release of special information not suitable for formal publication.

16. Abstract

Eleven semi-span wing models were tested in the 1/8-scale model of the Langley V/STOL tunnel to qualitatively study vortex bursting. Flow visualization was achieved by using helium filled soap bubbles introduced upstream of the model. The angle of attack range was from 0^{o} to 45^{o}.

The results show that the vortex is unstable, that is, the bursting point location is not fixed at a given angle of attack but moves within certain bounds. Upstream of the trailing edge, the bursting point location has a range of two inches; downstream, the range is about six inches. Anhedral and dihedral appear to have an insignificant effect on the vortex and its bursting point location.

Altering the section suction distribution by improving the triangularity of it, can generally increase the angle of attack at which vortex bursting occurs at the trailing edge.

17. Key Words (Suggested by Author(s)) (STAR category underlined)	18. Distribution Statement
Aircraft Vortex bursting Section suction distribution dihedral	Unclassified - Unlimited

19. Security Classif. (of this report)	20. Security Classif. (of this page)	21. No. of Pages	22. Price*
Unclassified	Unclassified	72	$4.25

*Available from { The National Technical Information Service, Springfield, Virginia 22151
STIF/NASA Scientific and Technical Information Facility, P.O. Box 33, College Park, MD 20740

ABSTRACT

Eleven semi-span wing models were tested in the 1/8-scale model of the Langley V/STOL tunnel to qualitatively study vortex bursting. Flow visualization was achieved by using helium filled soap bubbles introduced upstream of the model. The angle of attack range was from 0^{o} to 45^{o}.

The results show that the vortex is unstable, that is, the bursting point location is not fixed at a given angle of attack but moves within certain bounds. Upstream of the trailing edge, the bursting point location has a range of two inches; downstream, the range is about six inches. Anhedral and dihedral appear to have an insignificant effect on the vortex and its bursting point location.

Altering the section suction distribution by improving the triangularity of it, can generally increase the angle of attack at which vortex bursting occurs at the trailing edge.

SUMMARY

Eleven semi-span wing models were tested in the 1/8-scale model of the Langley V/STOL tunnel to qualitatively study vortex bursting. Flow visualization was achieved by using helium filled soap bubbles introduced upstream of the model. The angle of attack range was from 0° to 45°.

The results show that the vortex is unstable, that is, the bursting point location is not fixed at a given angle of attack but moves within certain bounds. Upstream of the trailing edge, the bursting point location has a range of two inches; downstream, the range is about six inches. Anhedral and dihedral appear to have an insignificant effect on the vortex and its bursting point location.

Altering the section suction distribution by improving the triangularity of it, can generally increase the angle of attack at which vortex bursting occurs at the trailing edge.

INTRODUCTION

The phenomenon of vortex bursting, presently under investigation at Langley Research Center, is an important consideration in strake, canard and wing design for aircraft utilizing vortex lift. Studies employing spanwise blowing to delay vortex bursting at the trailing edge to higher angles of attack have been conducted (Ref. 1, 2, 3). A cursory qualitative flow visualization study was conducted in the 1/8-scale model of the Langley V/STOL tunnel to determine the effect of dihedral, anhedral and section suction distribution (as controlled by planform shape) on vortex bursting. The visualization technique used helium filled soap bubbles as a means of illustrating the flow. The tests were conducted at a dynamic pressure of 1.5 lbs/ft^2 at an angle of attack from 0° to 45°.

SYMBOLS

b	wing span, m (ft)
c_s	leading-edge suction coefficient, $\frac{\text{Suction}}{q_\infty S_{ref}}$
c	local chord, m (ft)
q_∞	free-stream dynamic pressure, N/m^2 (lb/ft^2)
S_{ref}	reference area, m^2 (ft^2)
y	spanwise distance from root chord, m (ft)
α	angle of attack, deg
η	nondimensional spanwise coordinate $\left(\frac{2y}{b}\right)$

MODEL DESCRIPTION

Sketches of eleven semi-span models studied are presented in figures 1 to 8. Except for model VI, all the models were 0.25 inches thick and constructed of plexiglass or fiberglass. Model VI was made of brass plate and was 0.125 inches thick. Leading, trailing and side edges were sharp; the included angle of the bevel was 14° for all models except model VI. The included angle of the model VI bevel was 7°. For best photographic results, all models were painted a glossy black.

Models I, II and III (figure 1) were highly swept delta wings with leading edge sweep angles of 76° (aspect ratio of 1). Model I was flat while models II and III had circular arc dihedral and anhedral respectively. All three models had root chord lengths of 18.00 inches.

Models IV and V (figure 2) had a planform typical of a blended wing supersonic cruise fighter. Model IV was a flat plate model while model V had dihedral typical of that being considered as a means of providing directional stability for a supersonic cruise fighter.

The choice of planform shape for models VI to XI is related to the spanwise variation of attached flow leading-edge suction as explained in the discussion of the results.

Models VI and VII had curved leading-edge planforms with initial high and low leading-edge sweep angles respectively. Both had root chord lengths of 18.00 inches (figures 3 and 4).

Models VIII and IX were modifications of models VI and VII. Model VIII (figure 5) had an initial leading edge sweep of 76°. This sweep gradually decreased to 69° starting 12.6 inches from the apex. Model IX (figure 6) is model VII with the rectangular aft section starting 12.6 inches from the apex cut off. The root chord for this model was 12.6 inches.

The last two models, X and XI had planforms with an initial leading-edge sweep angle of 76°. The tips were then clipped causing an increase in the sweep of the leading edge. This change in leading edge sweep occurred at a semi-span distance of 3.9 inches and 3.13 inches from models X and XI respectively. (figures 7 and 8) The root chord length for these two models was 18.00 inches. A summary of model numbers and planforms can be found in table 1.

APPARATUS AND TEST PROCEDURE

This study was conducted in the 1/8-scale model of the Langley V/STOL tunnel. Tests were run at a dynamic pressure of 1.5 lbs/ft^2 which resulted in the best photographs. Since the seperation point is fixed by the sharp leading edges of the models, the low Reynolds number of the test should not significantly affect the flow field.

Mounting for the models consisted of a circular plexiglass disk, 18.00 inches in diameter, fitted into a backboard. This reflection plane (disk and backboard) was painted a glossy black. The white lines (distance markings) on the reflection plane along the root chord of the model were 2.0 inches apart with the first line 4.0 inches from the apex. White lines .5 inches apart were also placed spanwise on the models near

the trailing edge for some phases of the study.

The flow visualization was achieved through the use of a helium bubble generator and a specially designed nozzle which produced neutrally bouyant, helium filled, soap bubbles. The bubbles were introduced upstream of the model. When photographed, the bubbles appeared as white streaks. A high intensity light directed upstream was used to illuminate the bubbles. The white bubbles and glossy black of the models and reflection plane created a good contrast so that the vortices and their bursting points were easily visible.

Photographs were taken with a Hasselblad 500 EL/M camera. The pictures were taken at a shutter speed of 1/8 of a second and an f-stop setting of 5.6. The film used was 70 mm. Kodak Tri-X Pan ASA 400. The ASA rating was then increased to ASA 1000 through special development processes. The angle of attack range of the photographs was from 15° to 45°.

DISCUSSION OF RESULTS

The purpose of this flow visualization study was to qualitatively investigate the effect of anhedral or dihedral on the location of the bursting point of the primary vortex. In addition, a flow study to determine the effect of the theoretical spanwise section suction distribution on the primary vortex was conducted. It has been suggested in reference 4 that the theoretical spanwise section suction distribution is one of the parameters that determines the vortex breakdown characteristics.

The choice of the planform shapes for the section suction distribution study will be explained later in this discussion.

Figure 9 is a representative close-up of the core and bursting point of a primary vortex using model IV at a 40° angle of attack. Subsequent photographs will include distance marks on the reflection plane, and, in some cases, also on the semi-span.

In most cases, the vortices were extremely strong producing a definite vortex core. By decreasing the size of the soap bubbles, the weaker and smaller secondary vortices were also visible.

In studying the photographs, the reader should be alert to reflections from the glossy surfaces of both the model and reflection plane. Although care was taken to obtain the clearest possible pictures, removal of all reflections was impossible. Further, the camera angle changes somewhat between different angles of attack and models. Because of this, the distance markings can give only general vortex locations. In all photographs used, a definite core or bursting point does appear.

Results of the study in general show that the vortex bursting point is not stable but does change a significant amount in a short period of time. Upstream of the trailing edge, the range in location is about two inches (figure 10). Downstream of the trailing edge, the range is much greater - approximately six inches. Due to the bursting point instability, a series of pictures were taken for each angle of attack and model to try and obtain a picture representing the average. Since the bursting points move as discussed above, the locations of the bursting points should be considered as approximate.

The Dihedral-Anhedral Effect

Models I through V were considered in this part of the study. Some representative flow visualization pictures showing bursting on wings with anhedral and dihedral are presented in figures 11 to 38.

1. Delta Wing (aspect ratio of 1) - Models I, II and III

a) ALPHA = 31° Figures 11 through 13 present models I, II and III respectively. All three models exhibit a strong vortex core with no bursting point upstream of the trailing edge. Each model also showed a secondary vortex along the leading edge. In figure 14, this secondary vortex is clearly visible on model I. The position of the primary core and the spiral flow around it is barely visible.

b) ALPHA = 32° Vortex bursting is first visible at or near the trailing edge at 32°. Figure 15 shows bursting for model I approximately 16 inches from the apex. In figure 16, bursting occurs at 17 inches on model II while figure 17 shows no bursting for model III. In figure 18, however, the bursting point for model III can barely be seen at 17 inches. This is not suprising, for, as mentioned earlier, the bursting point is unstable and tends to move as figures 17 and 18 indicate. Most of the bubbles in figure 18 are contained in the secondary flow along the leading edge. It is interesting to note that this secondary flow appeared to be stronger on model III than on either model I or II.

c) ALPHA = 35° The flow fields for models I, II and III at an angle of attack of 35° are presented in figures 19 through 21.

The bursting point for model I at this angle is about 13 inches from the apex and 12 inches for model II. For model III, the bursting point is 10 inches.

d) ALPHA = 40° Figures 22, 23, and 24 present models I, II and III respectively at 40° angle of attack. Bursting points for models I and II are approximately 6 inches from the apex while model III is about 7 inches.

e) ALPHA = 45° Models I, II and III are at 45° angle of attack in figures 25 through 27. At this angle of attack, all three bursting points were less than 4 inches from the apex. Because of the rapid bursting and closeness to the apex, a more accurate location is not possible.

From the qualitative information presented in these photographs (figures 11-27) there appears to be no measurable effect of anhedral or dihedral on the primary vortex bursting point location for these wings.

2. Supersonic Cruise Fighter - Models IV and V

Pictures of the flow fields of models IV and V (whose planforms are typical of a supersonic cruise fighter) are presented in figures 28 to 38. The angle of attack range is from 15° to 45°.

a) ALPHA = 15° Model V in figure 28 shows the tightly coiled leading-edge vortex originating on the curved portion of the wing as well as a trailing-edge vortex coming off the swept portion of the trailing edge. On model IV (figure 29) the leading-edge vortex is shown, while the trailing edge vortex is not visible. For both models, a primary vortex off the apex does exist although it is not shown in these figures.

b) ALPHA = 25° Figure 30 shows the direction of spin of the trailing-edge vortex on model IV. It is spinning counter-clockwise; that is, the flow is from the lower surface to the upper surface. This direction of spin is also the same on model V.

c) ALPHA = 30° Figure 31 and 32 show the core of the primary vortex for models IV and V respectively. On both models (although it is easier to see in figure 31) the core re-aligns with the free stream as expected.

d) ALPHA = 35° For both models IV and V (figures 33 and 34) the primary vortex bursts at or near the trailing edge at an angle of attack of 35°. At lower angles of attack, all bursting points are downstream of the trailing edge.

e) ALPHA = 40° Figures 35 and 36 show models IV and V at 40° angle of attack. Both bursting points are about 9 inches from the apex.

f) ALPHA = 45° Models IV and V are shown in figures 37 and 38 at an angle of attack of 45°. Here again, there is little difference between the two models. Both bursting points are located approximately 6 inches from the apex. Between these two models, little difference in bursting point location was expected after the bursting point attained a location of 12 inches from the apex since the models are geometrically identical from 0 to 12 inches.

As with the delta wing, the dihedral in the outboard section did not affect the vortex bursting. This was expected since the primary vortex is basically rolled up from the highly swept portion of the wing. Closer

examination of the outboard leading-edge vortex is required before the effect of dihedral on its bursting point can be determined.

Effect of Section Suction Distribution on Vortex Bursting

The second part of the flow visualization study involved the effect of various planform shapes on section suction distribution. Flow studies were conducted over an angle of attack range of 0° to 45°. Bursting point locations downstream as well as upstream of the trailing edge were studied.

In reference 4, Lamar points out that one of the parameters affecting leading-edge vortex bursting is the theoretical attached flow spanwise distribution of section leading-edge suction distribution (c_s c/2b) which can be controlled by planform changes. Triangulating this distribution delays vortex bursting at the trailing edge until higher angles of attack are reached. Figure 39 presents the section suction distribution for a series of four delta wings. It can be seen that the lower aspect ratio delta wing has the more triangular distribution. It should be noted that the more highly swept, lower aspect ratio wing can attain a higher angle of attack before vortex bursting occurs at the trailing edge (ref. 5). For this series and all succeeding wings, the sectional suction distribution is determined by the use of the vortex lattice program of reference 6. Vortex bursting studies involving several wing shapes (figure 40) were conducted by Earnshaw (ref. 7). The section suction distribution for these wings were obtained and are presented in figure 41. The section suction values are presented in table 2.

Figure 42 shows Earnshaw's experimental results. It is interesting to note that for wing 4E which has an increased leading-edge sweep beginning at a semi-span distance of 3.2757 inches, the section suction distribution becomes more triangular than that of wing 3E, which had a constant leading-edge sweep. The same effect is seen between wing 2E and 1E. The experimental results indicate that wing 4E (The most triangular sectional suction distribution) has the highest angle of attack for vortex bursting at the trailing edge. As the leading-edge sweep of wing 4E approaches that of wing 3E (moving from the trailing edge to the apex), little difference in bursting point locations for the two models is seen.

In an attempt to verify that the section suction distribution is an important parameter for leading-edge vortex bursting, models I, VI, VII, VIII, IX, X and XI were constructed and tested.

The section suction distribution and experimental results for model I (the delta wing) are shown in figure 43 and 44 respectively. Results for models X and XI (the clipped wing models) are also shown in these figures.

Figure 43 presents the section suction distribution for models I, X and XI. Of these three, model XI has the most triangular shape. Table 3 presents the section suction values for these three models.

The experimental results (figure 44) indicate that for models X and XI, a slightly higher angle of attack can be reached before the vortex bursts at the trailing edge than for model I. Between models X and XI,

there is a negligible difference in the angle of attack at which the vortex bursts at the trailing edge.

The sectional suction results for models VII and IX are shown in figure 45. It should be noted that the side-edge section suction contribution is not included in the values at the tip. The section suction values for models VII and IX are presented in table 4.

The experimental results for models VII and IX in figure 46 show that the angle of attack for the trailing edge bursting is significantly lower for models VII and IX, than for I, X and XI. Comparison between models VII and IX show trends different from those observed for other models. Those results showed that for the more triangular section suction distributions with high suction values (better triangular distributions), a higher angle of attack could be reached before vortex bursting occurred at the trailing edge. Based on the sectional suction distribution it would appear then, that model IX would attain a higher angle of attack before bursting occurred at the trailing edge. But, as mentioned above experimental results show that model VII attains the higher angle of attack (21°) than model IX (20°). From these two models, it appears that the streamwise side-edge vortex of model VII delays bursting at the trailing edge.

Some interesting photographs of model VII at 20° angle of attack are shown in figures 47 and 48. Figure 47 shows the tightly coiled primary vortex core. Figure 48 shows the same primary core which appears to be formed of two cores with two bursting points. Also visible is the secondary vortex along the leading edge.

Presented in figures 49 and 50 are the section suction distribution and flow visualization results for models VI and VIII. The section suction distribution (figure 49) of model VI shows a high peak at $\eta = .1$. This early peak is due to the high inboard leading-edge sweep. The rather drastic change in the leading-edge sweep, which causes the sudden decrease in section suction values after $\eta = .1$, also causes the vortex to roll up on the inboard portion of the wing only. It would be expected, based on the $c_s\ c/2b$ distribution from $\eta = 0.$ to $\eta = .1$ that the vortex associated with the inboard part of the wing would be strong and not burst at the trailing edge until reaching higher angles of attack. Figure 50 shows that this is true. The bursting point for model VI does not reach the trailing edge until the angle of attack is 38°.

The section suction distribution for model VIII (figure 49) is shifted slightly to the right with a lower peak value than model VI. As can be seen, the angle of attack at which the vortex bursts for model VIII is nearly the same as those for models I, X and XI (figure 43).

Some interesting results have been obtained from this study, but the flow visualization technique used may not give the refinement and detail necessary for a quantitative study of this sort.

CONCLUDING REMARKS

Eleven semi-span wing models were tested in the 1/8-scale model of the Langley V/STOL tunnel qualitatively study vortex bursting. Flow visualization was achieved by using helium filled soap bubbles introduced upstream of the model. The angle of attack range was from 0° to 45°. A summary of the major results follows below.

1) The vortex is unstable, that is, the bursting point location is not fixed. Upstream of the trailing edge, it has a range of 2 inches; downstream, the range is about 6 inches.

2) Anhedral and dihedral appear to have an insignificant effect on the vortex and its bursting point location.

3) Altering the section suction distribution by improving the triangularity of it, can generally increase the angle of attack at which vortex bursting occurs at the trailing edge.

REFERENCES

1. Bradly, R. O., and Wray, W. O.: A Conciptual Study of Leading Edge Vortex Enhancement by Blowing. AIAA Paper No. 73-656, July 1973.

2. Scantling, W. L., and Gloss, B. B.: Effect of Spanwise Blowing on Leading-Edge Vortex Bursting of a Highly Swept Aspect Ratio 1.18 Delta Wing. NASA TM X-71987, 1974.

3. Erickson, Gary E.: Flow Visualization of Trapped Vortices Enhanced by Spanwise Blowing. 1975 AIAA Middle Atlantic Conference.

4. Lamar, John E.: Some Recent Applications of the Suction Analogy to Vortex-Lattice Estimates. Proposed NASA SP, 1975.

5. Polhamus, Edward C.: Predictions of Vortex-Lift Characteristics by a Leading-Edge Suction Analogy. J. Aircraft, vol. 8: no. 4, April 1971, pp. 193-199.

6. Margason, Richard J., and Lamar, John E.: Vortex-Lattice Fortran Program for Estimating Subsonic Aerodynamic Characteristics of Complex Planforms. NASA TN D-6142, 1971.

7. Earnshaw, P. B.: Measurements of Vortex Breakdown Position at Low Speed on a Series of Sharp-Edged Symmetrical Models. C. P. No. 828, 1965.

MODEL	PLANFORM	
I	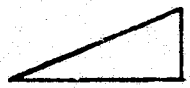	
II	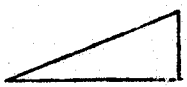	(dihedral)
III	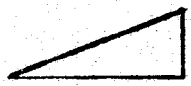	(anhedral)
IV		
V	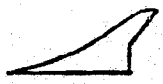	(dihedral)
VI		
VII	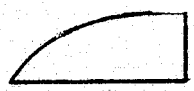	
VIII	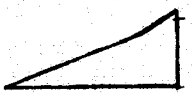	
IX	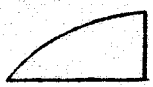	
X	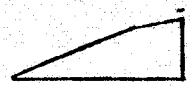	
XI		

TABLE 1. SUMMARY OF MODEL PLANFORMS AND NUMBERS

MODEL 1E		MODEL 2E		MODEL 3E	
η	c_s c/2b	η	c_s c/2b	η	c_s c/2b
.96667	.11438	.99722	1.45594	.96667	.39873
.90000	.15057	.98704	1.33610	.90000	.49259
.83333	.16247	.96752	1.10638	.83333	.52006
.76667	.16291	.93879	.76821	.76667	.50669
.70000	.15716	.90127	.52689	.70000	.47411
.63333	.15820	.85544	.44097	.63333	.48316
.56667	.15613	.81664	.43171	.55667	.47319
.50000	.14909	.78800	.39156	.50000	.44477
.43333	.13890	.74130	.36047	.43333	.48794
.36667	.12666	.67480	.33277	.36667	.36767
.30000	.11260	.60691	.32182	.30000	.32390
.23333	.09632	.54024	.30533	.23333	.27347
.16667	.07928	.47358	.28230	.16667	.22562
.10000	.06352	.40691	.26309	.10000	.18482
.03333	-.07482	.34024	.23654	.03333	-.28367
		.27358	.20142		
		.20691	.17713		
		.14024	.14683		
		.07358	.06405		
		.02012	-.50287		

TABLE 2.- SECTION SUCTION VALUES - EARNSHAW MODELS

MODEL 4E		MODEL 5E	
η	c_s c/2b	η	c_s c/2b
.99256	3.80777	.99882	1.43485
.97293	3.30929	.99279	1.36226
.94404	2.57530	.96957	1.08247
.90631	1.82710	.91636	.44472
.86022	1.40733	.84821	.35071
.82120	1.41810	.79680	.34522
.79240	1.31458	.74540	.29912
.74543	1.16258	.68303	.29968
.67837	1.08577	.62066	.29371
.61010	1.00844	.55752	.28917
.54343	.95185	.49037	.29462
.47676	.88980	.42120	.30457
.41010	.81199	.36960	.31472
.34343	.70924	.31648	.29588
.27676	.62208	.24981	.24557
.21010	.54080	.18314	.20594
.14343	.45663	.11648	.17106
.07676	.17147	.04157	-.27821
.02171	-1.66738		

TABLE 2.- (Con't)

MODEL I		MODEL X		MODEL XI	
η	c_s c/2b	η	c_s c/2b	η	c_s c/2b
.96667	1.25931	.96739	2.99448	.94523	11.32181
.90000	1.45728	.90101	2.78105	.85200	4.86469
.83333	1.47252	.82877	1.99829	.77508	2.85466
.76667	1.43604	.75185	1.73883	.69816	2.91095
.70000	1.38639	.67493	1.64575	.62123	2.73104
.63333	1.27991	.59800	1.53198	.54431	2.45279
.56667	1.19983	.52108	1.41319	.46739	2.12566
.50000	1.11922	.44416	1.25128	.39046	1.79689
.43333	.99804	.36723	1.05498	.31354	1.51659
.36667	.85472	.29031	.84335	.23662	1.27481
.30000	.69917	.21339	.64502	.15970	.99202
.23333	.54726	.13647	.51156	.08277	.37341
.16667	.41537	.04900	.01546	.02216	-.41779
.10000	.27971				
.03333	.01235				

TABLE 3.- SECTION SUCTION VALUES - MODELS I, X, AND XI

MODEL VII		MODEL IX	
η	c_s c/2b	η	c_s c/2b
.97628	2.35697	.97628	2.77900
.90743	1.22474	.90743	1.51112
.82898	.99735	.82898	1.21873
.77383	.91055	.77383	1.15995
.71868	.77784	.71868	1.04429
.65852	.67394	.65852	.91254
.59836	.59697	.59836	.75938
.52115	.52246	.52115	.61150
.44395	.41619	.44395	.48225
.37728	.36121	.37728	.44737
.31235	.32119	.31235	.39809
.24742	.23560	.24742	.29072
.18075	.18906	.18075	.23354
.11409	.15819	.11409	.19519
.04038	-.10373	.04038	-.02353

TABLE 4.- SECTION SUCTION VALUES - MODELS VII AND IX

MODEL VI		MODEL VIII	
η	c_s c/2b	η	c_s c/2b
.96429	.42440	.96429	.48171
.89286	.64382	.89286	.62015
.82143	.74513	.82143	.75385
.75029	.84996	.75893	.75744
.67915	1.00555	.68268	.91127
.60772	1.02284	.59750	.91937
.53701	1.09620	.52607	.82434
.46629	1.25499	.45464	.73061
.39601	1.26147	.38321	.65494
.30924	1.32125	.31179	.55439
.21888	1.30480	.24036	.43881
.15060	1.21680	.16893	.31360
.10040	1.31728	.09750	.17006
.06024	.66840	.03089	-.01651
.02008	.01216		

TABLE 5.- SECTION SUCTION VALUES - MODELS VI AND VIII

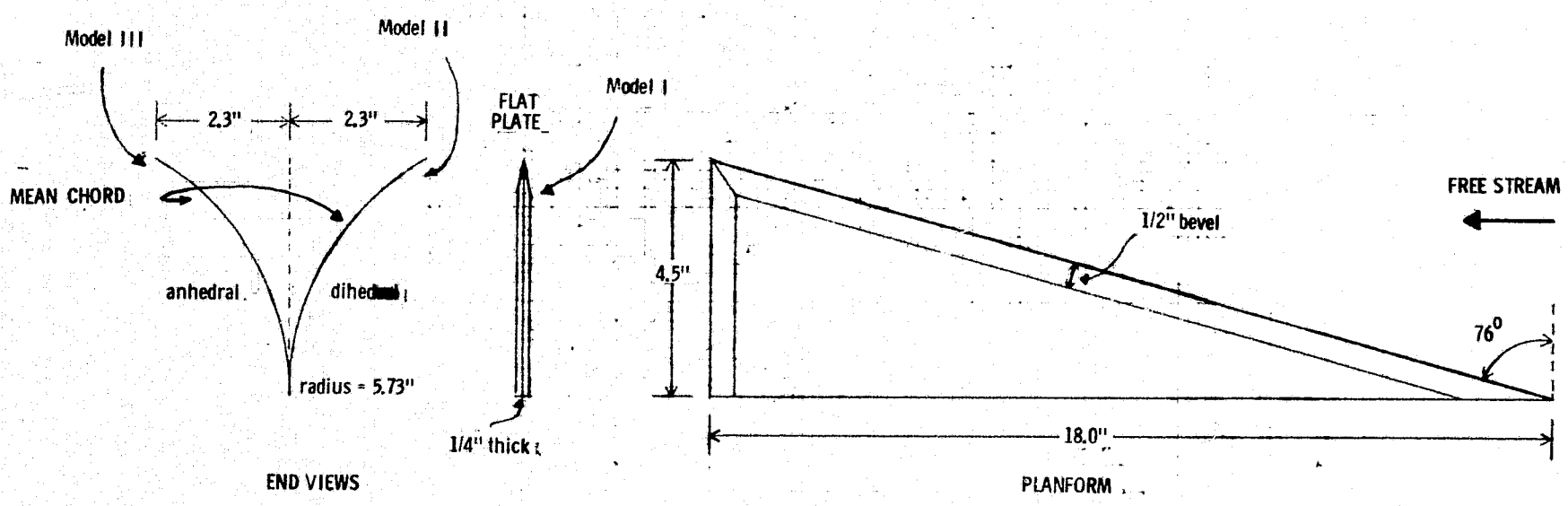

FIGURE 1. SKETCH OF MODELS I, II and III

STATION	COORDINATES X' (in)	Y' (in)
a	5.0	1.3
b	4.5	.7
c	4.0	.4
d	3.5	.1

STATION	COORDINATES X (in)	Y (in)
A	2.15	.395
B	4.30	.72
C	6.45	.99
D	8.60	1.39
E	10.00	1.70
F	10.90	2.00
G	11.60	2.20
H	13.00	3.00
I	14.00	3.70
J	14.85	4.20
K	16.20	4.70
L	17.30	4.90

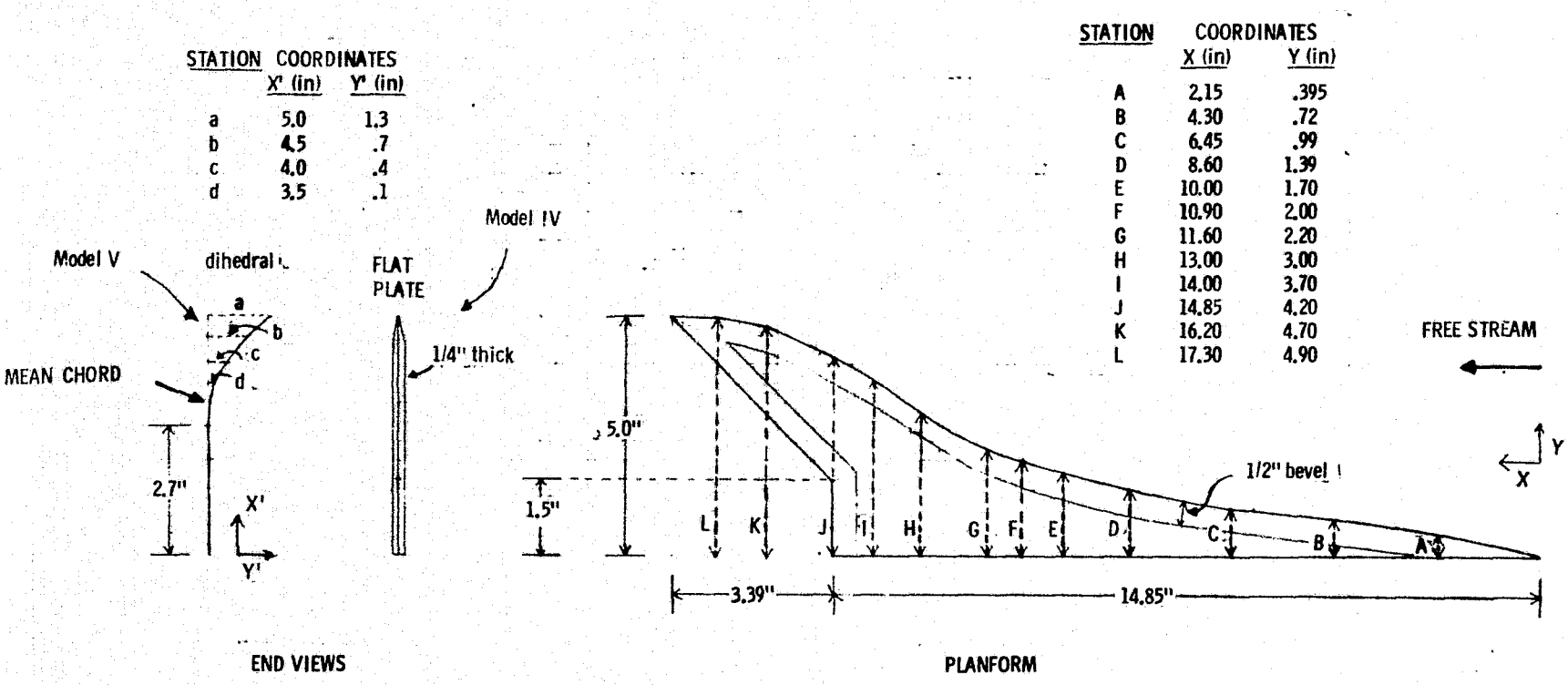

FIGURE 2. SKETCH OF MODELS IV AND V

POINT	X (in)	Y (in)
A	3.6	.18
B	5.4	.36
C	7.2	.54
D	9.0	.81
E	10.8	1.15
F	12.6	1.62
G	14.4	2.25
H	16.2	3.20

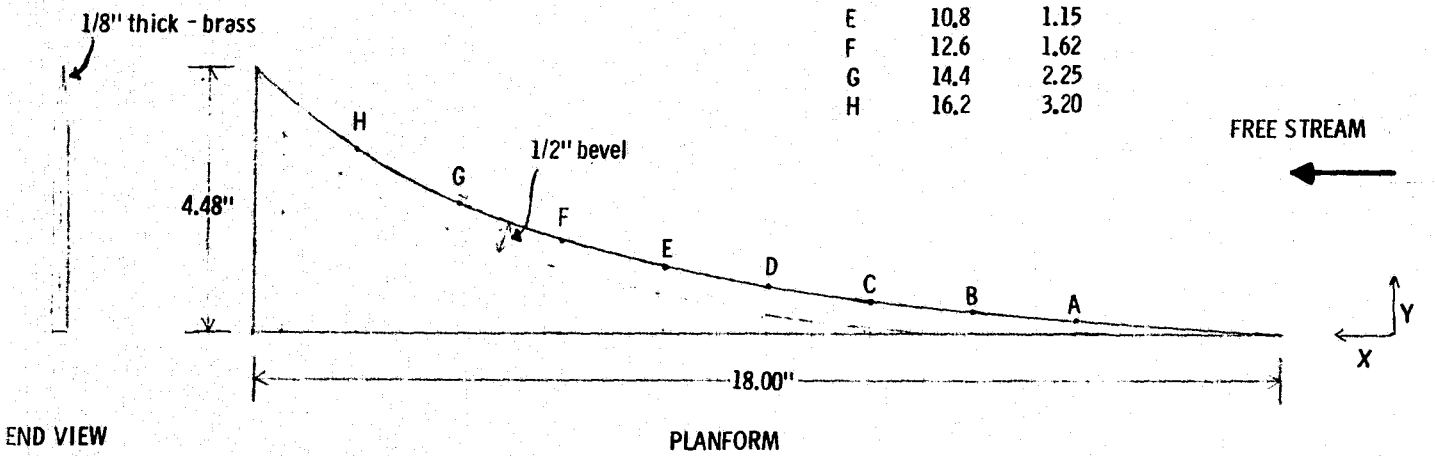

FIGURE 3. SKETCH OF MODEL VI

POINT	X (in)	Y (in)
A	1.8	1.260
B	3.6	2.140
C	5.4	2.835
D	7.2	3.375
E	9.0	3.870
F	10.8	4.275
G	12.6	4.480

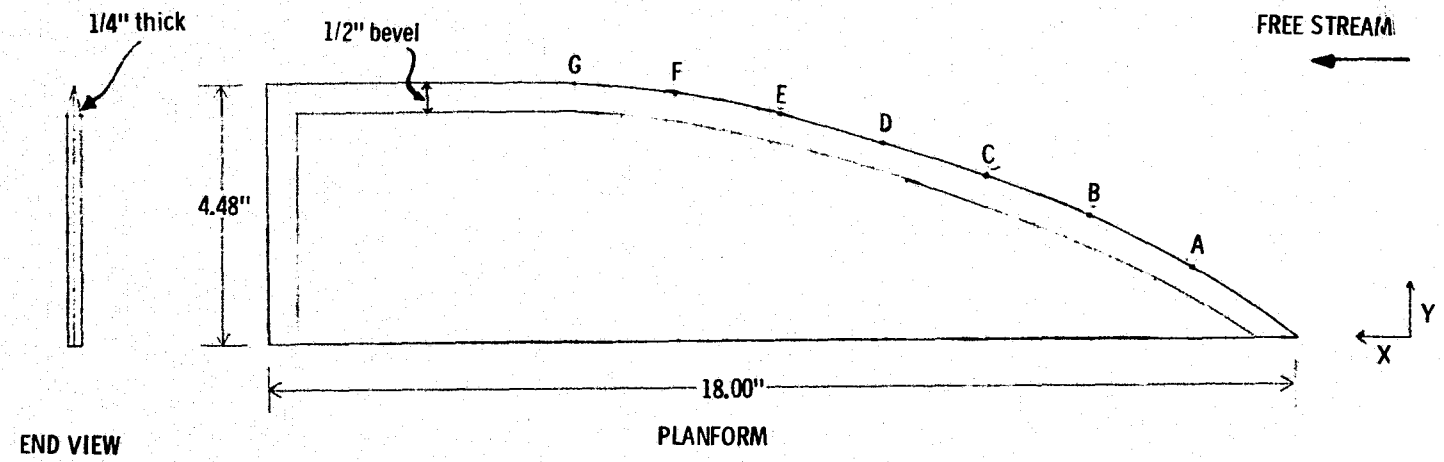

FIGURE 4. SKETCH OF MODEL VII

POINT	X(in.)	Y(in.)
A	12.6	3.19
B	14.4	3.69
C	16.2	4.32

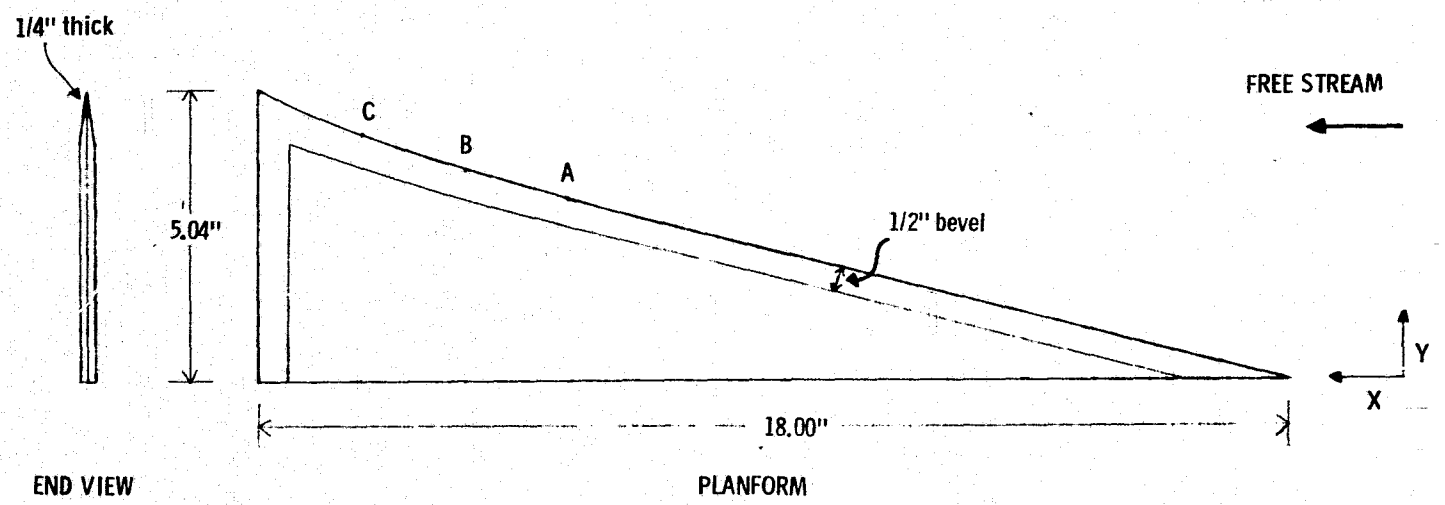

Figure 5. Sketch of Model VIII

POINT	X(in.)	Y(in.)
A	1.8	1.26
B	3.6	2.14
C	5.4	2.835
D	7.2	3.375
E	9.0	3.870
F	10.0	4.275

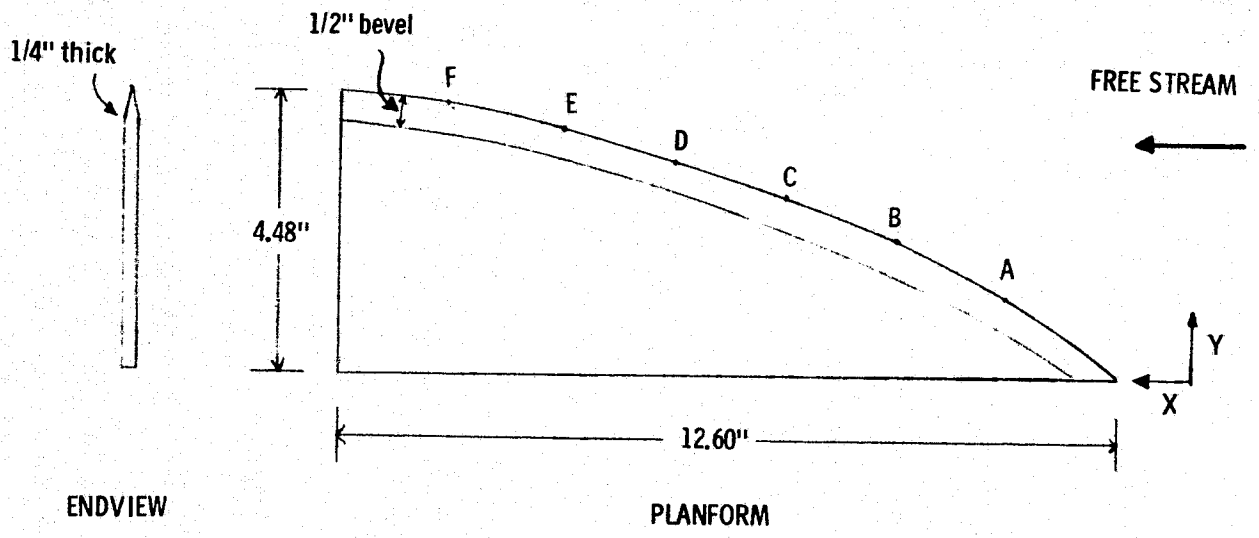

Figure 6. Sketch of Model IX

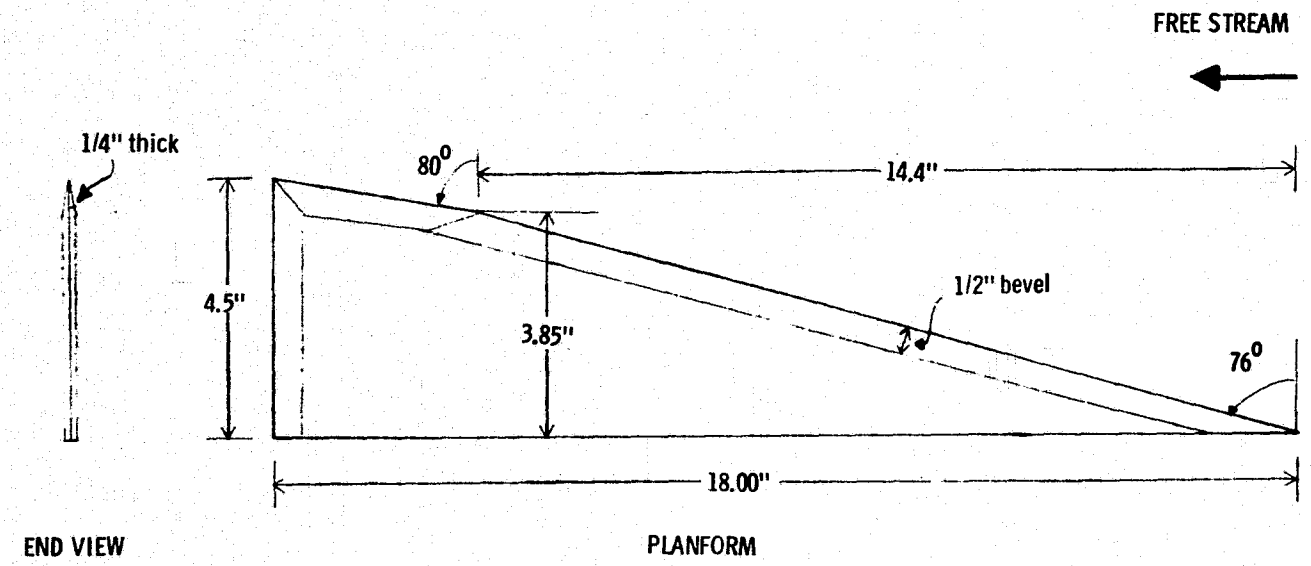

FIGURE 7. SKETCH OF MODEL X

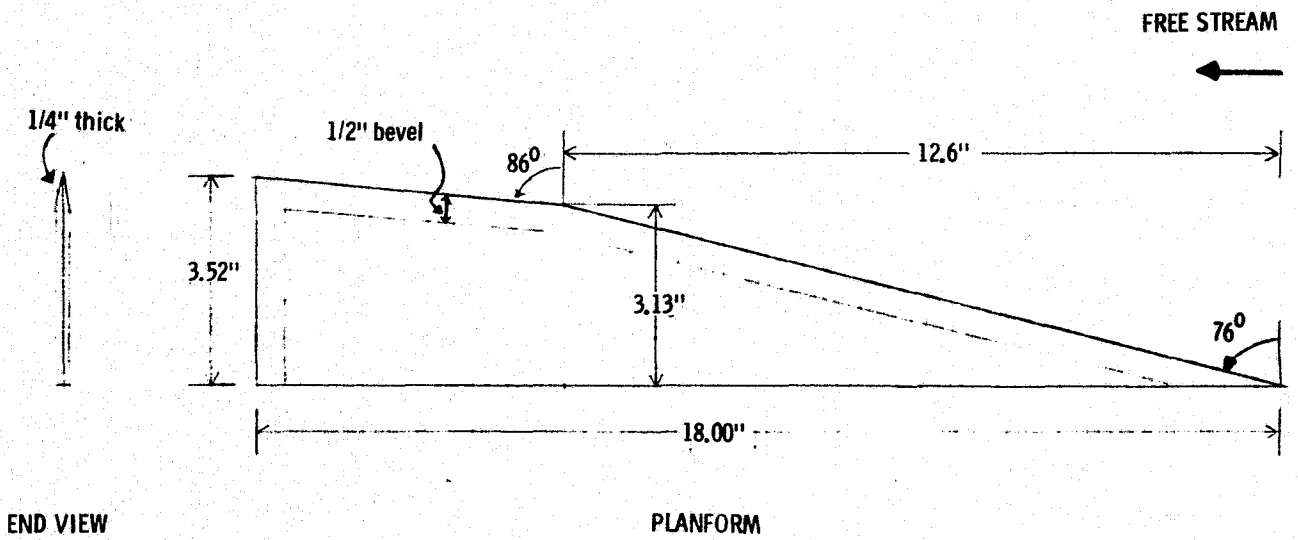

FIGURE 8. SKETCH OF MODEL XI

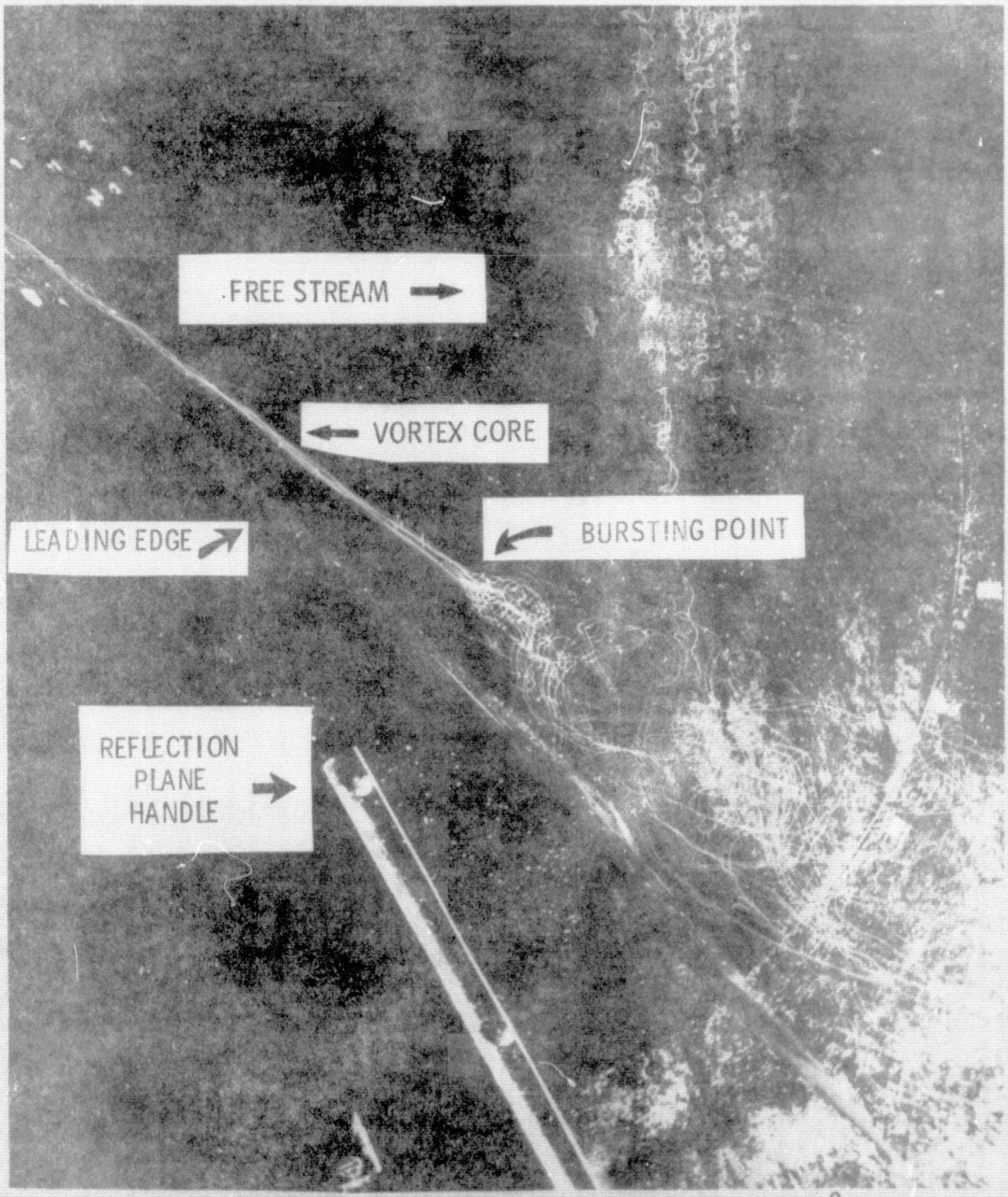

Figure 9. Close-up of primary vortex - Model IV at 40° angle of attack

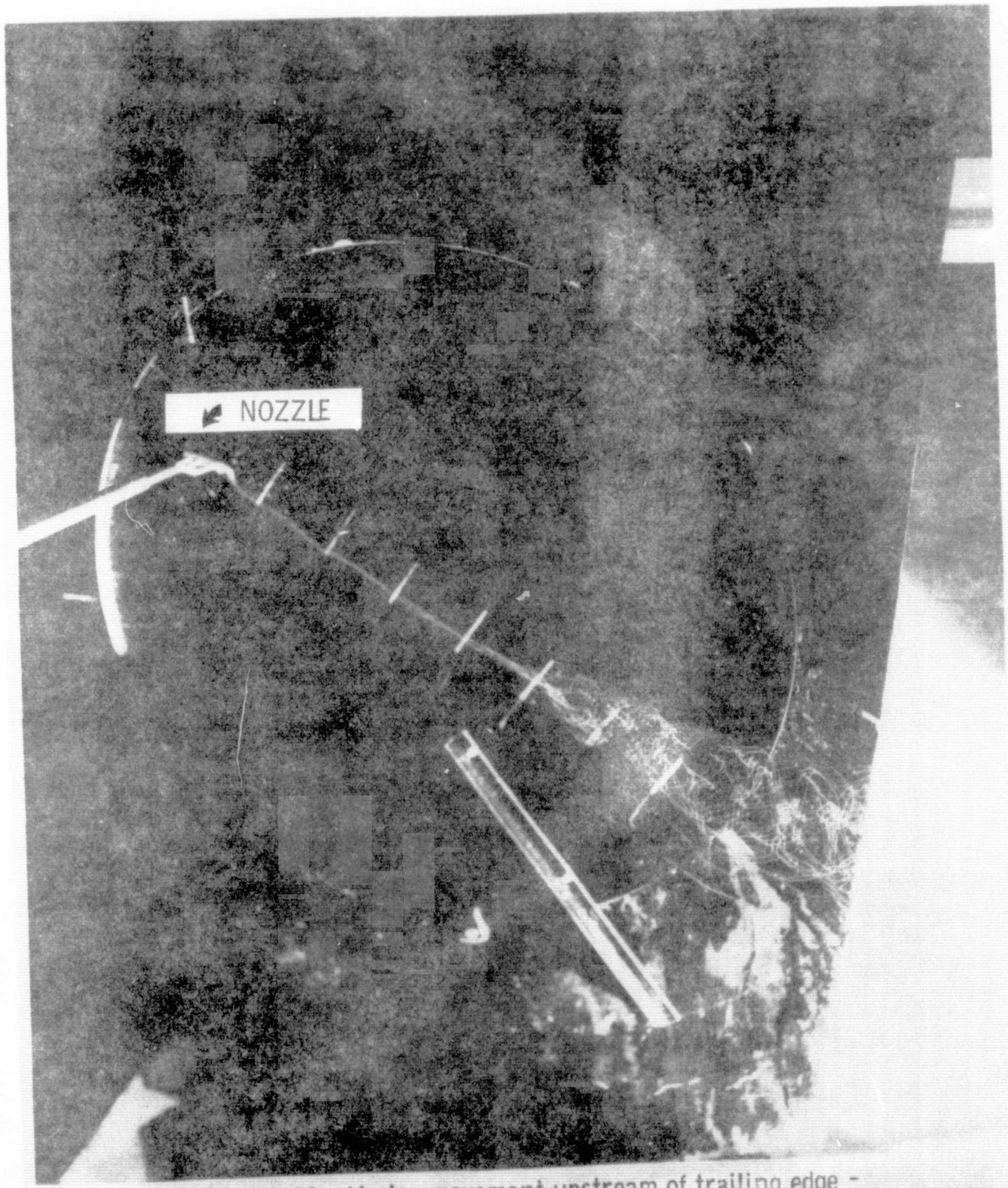

Figure 10. Vortex movement upstream of trailing edge - Model II at 35^{0} angle of attack

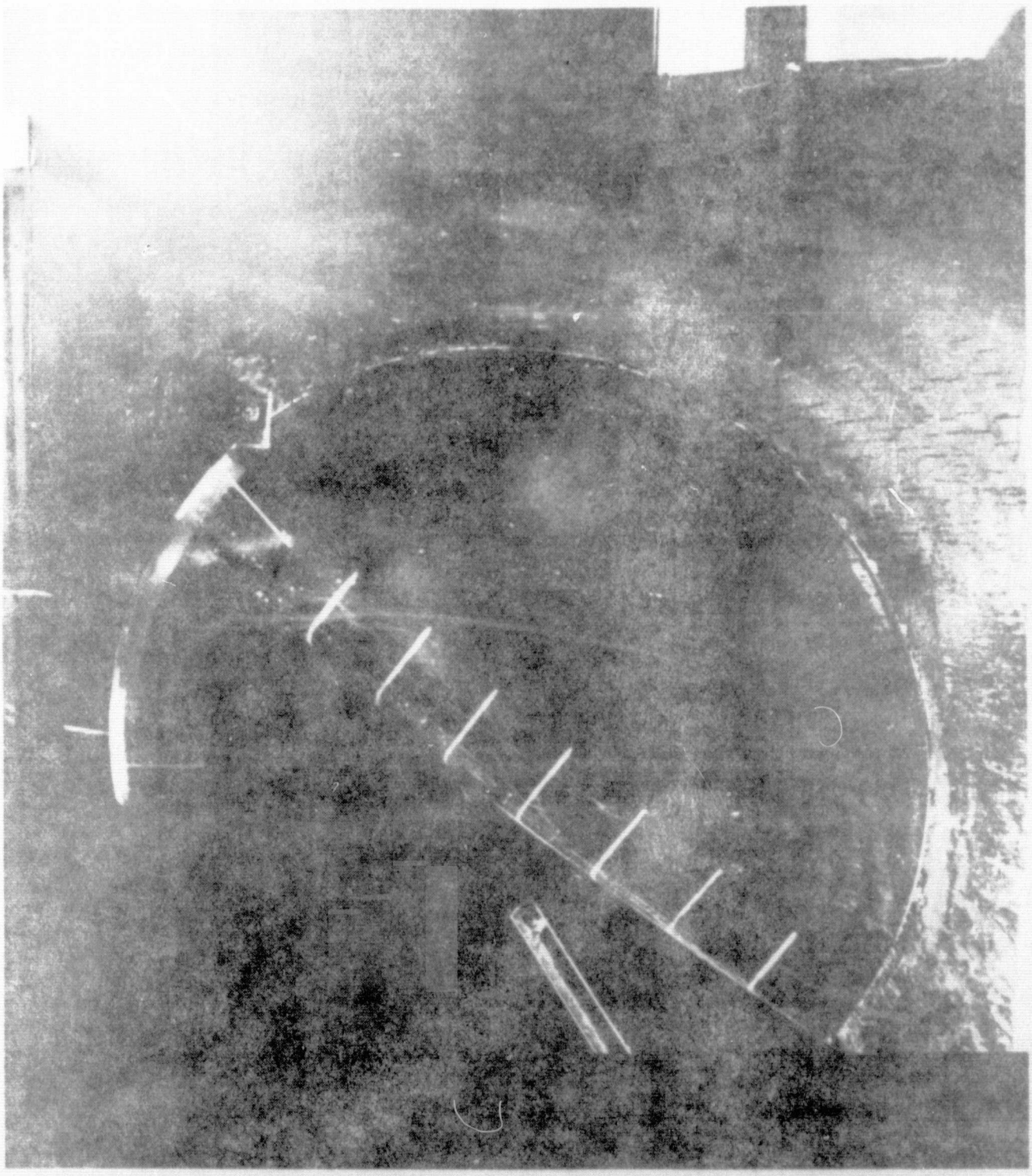

Figure 10. (Concluded) Model II at 35° angle of attack

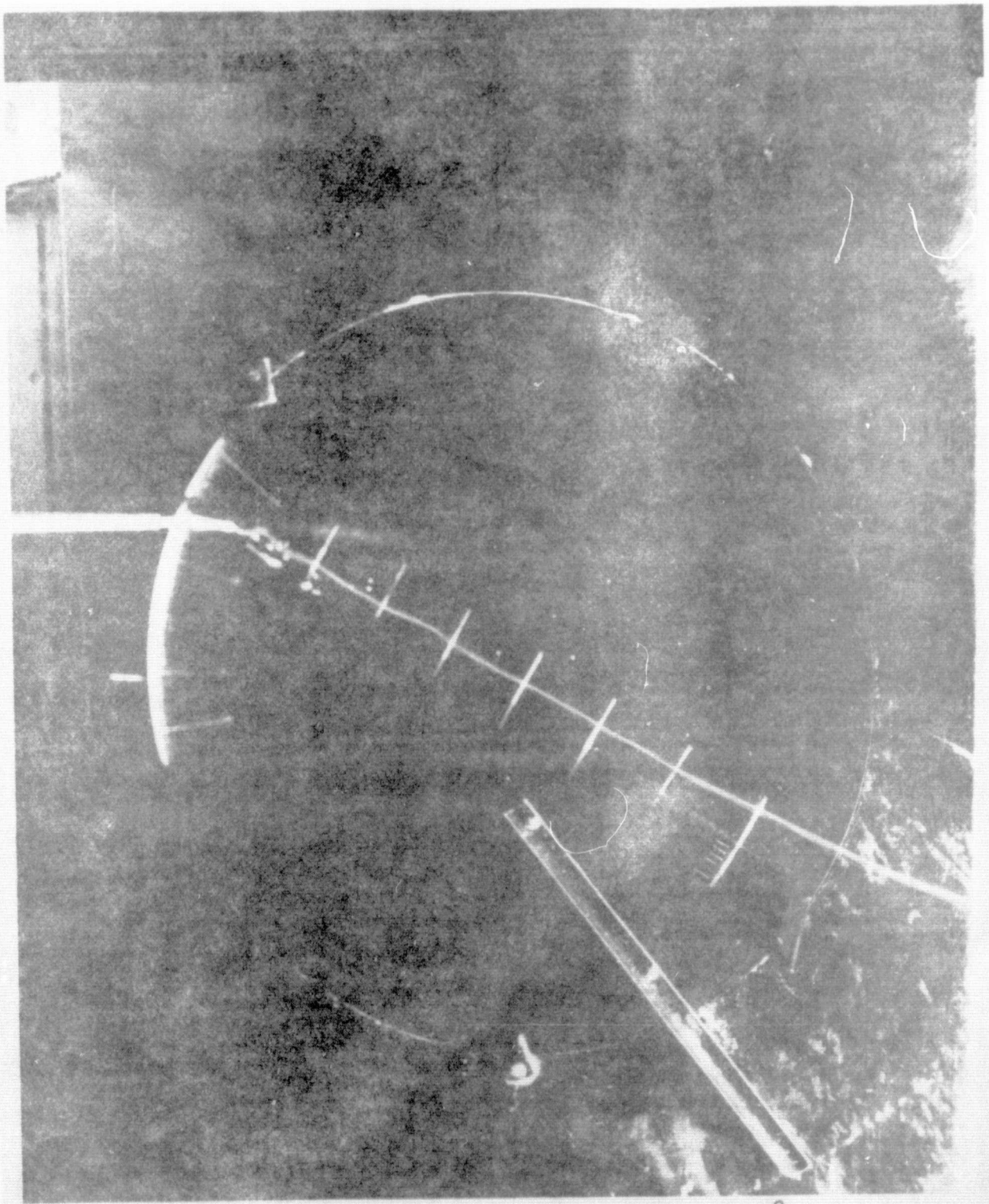

Figure 11. Primary vortex core of Model I at 31° angle of attack

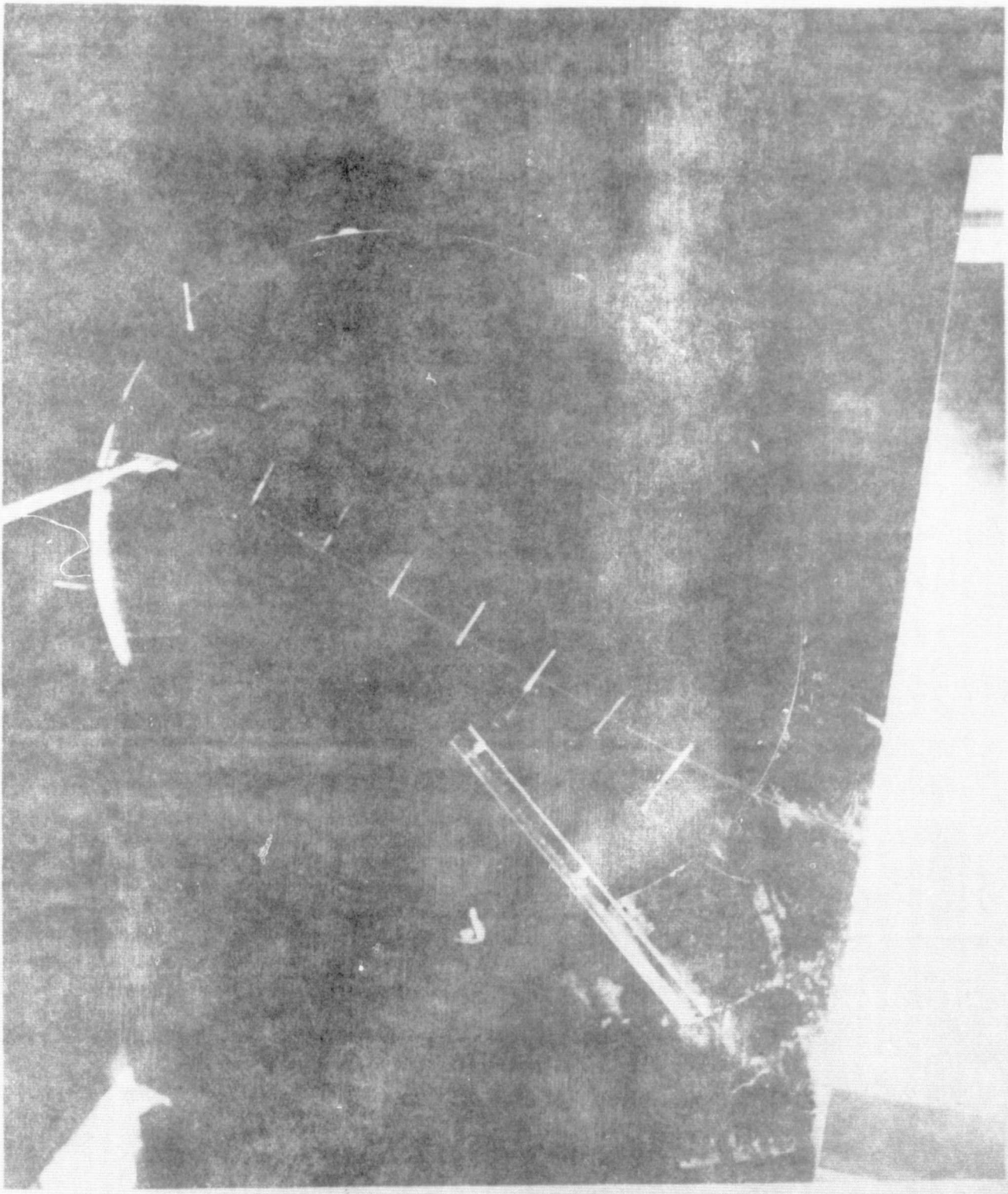

Figure 12. Primary vortex core of Model II at 31° angle of attack

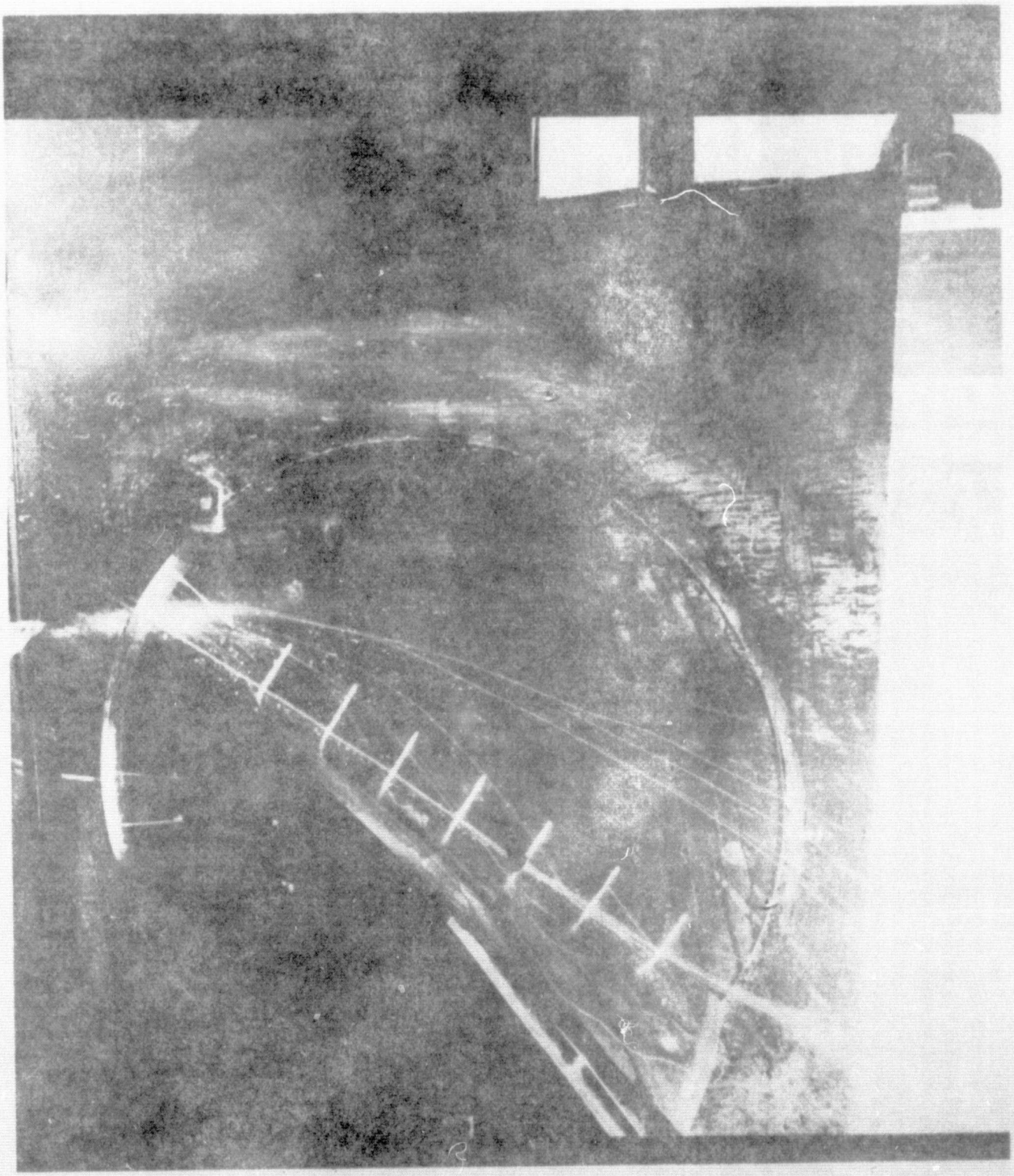

Figure 13. Primary vortex core of Model III at 31^{0} angle of attack

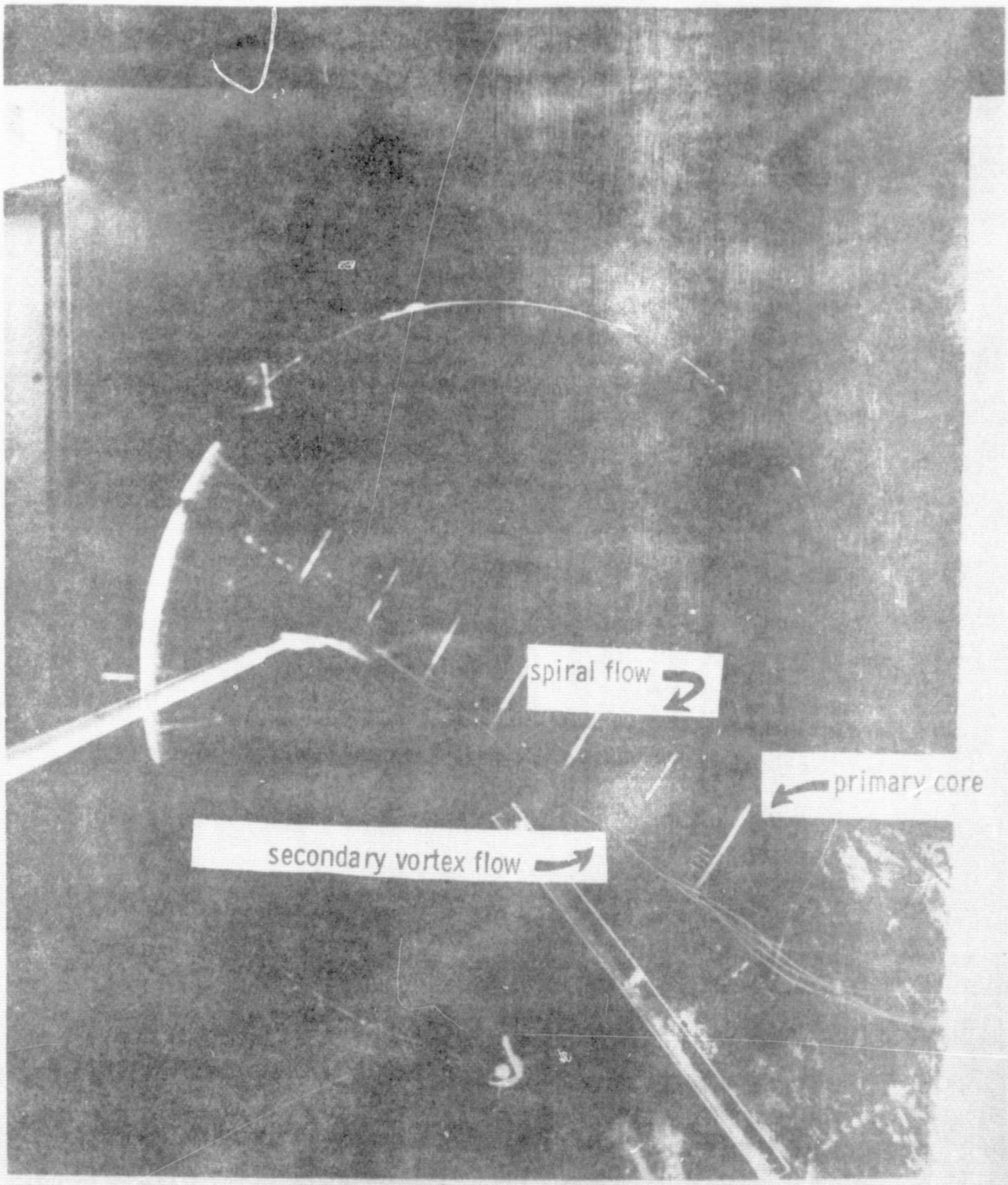

Figure 14. Secondary vortex of Model I at 31^{0} angle of attack

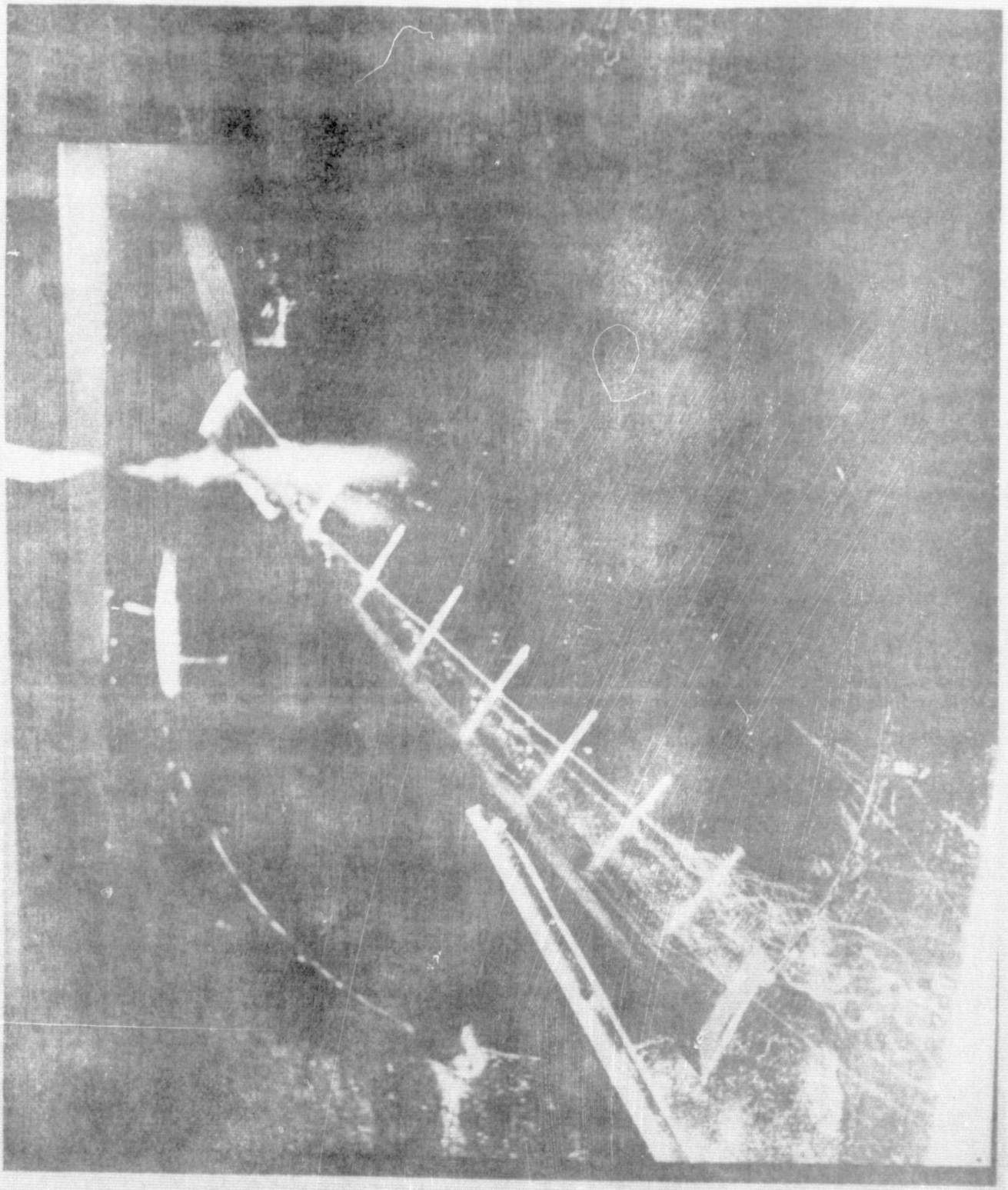

Figure 15. Vortex bursting near trailing edge - Model I at 32^0 angle of attack

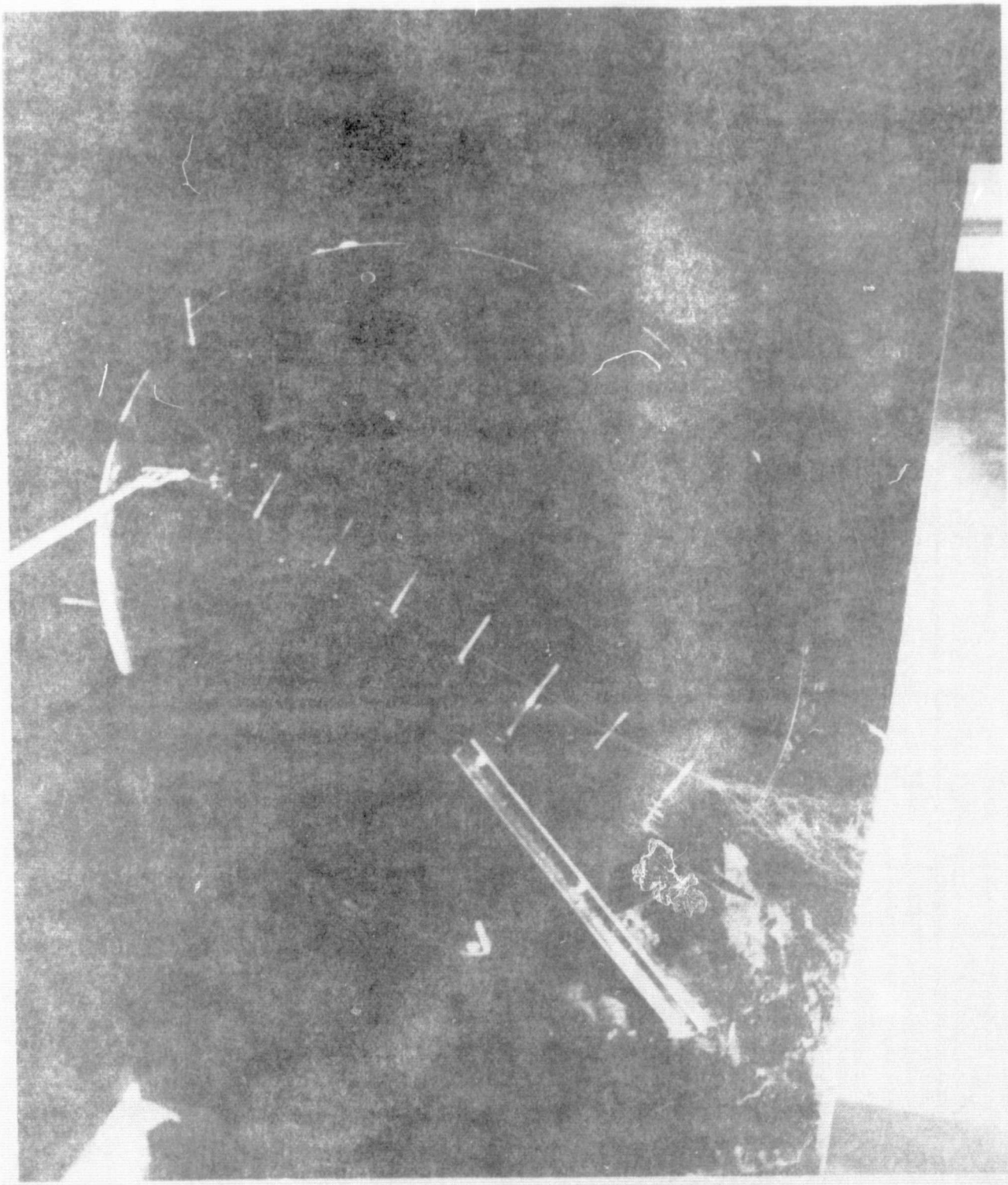

Figure 16. Vortex bursting at trailing edge for Model II at 32^0 angle of attack

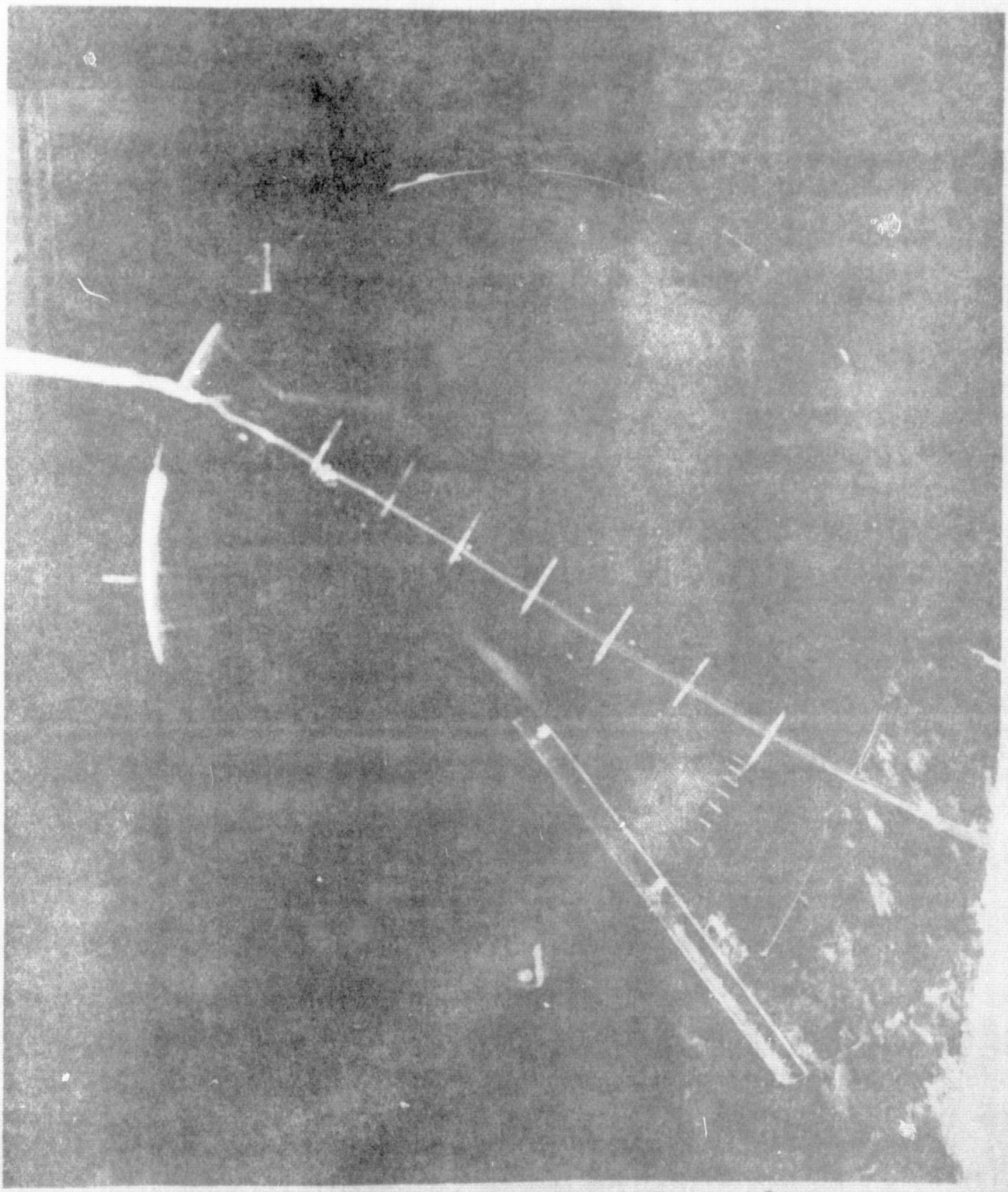

Figure 17. Primary vortex core of Model III at 32° angle of attack

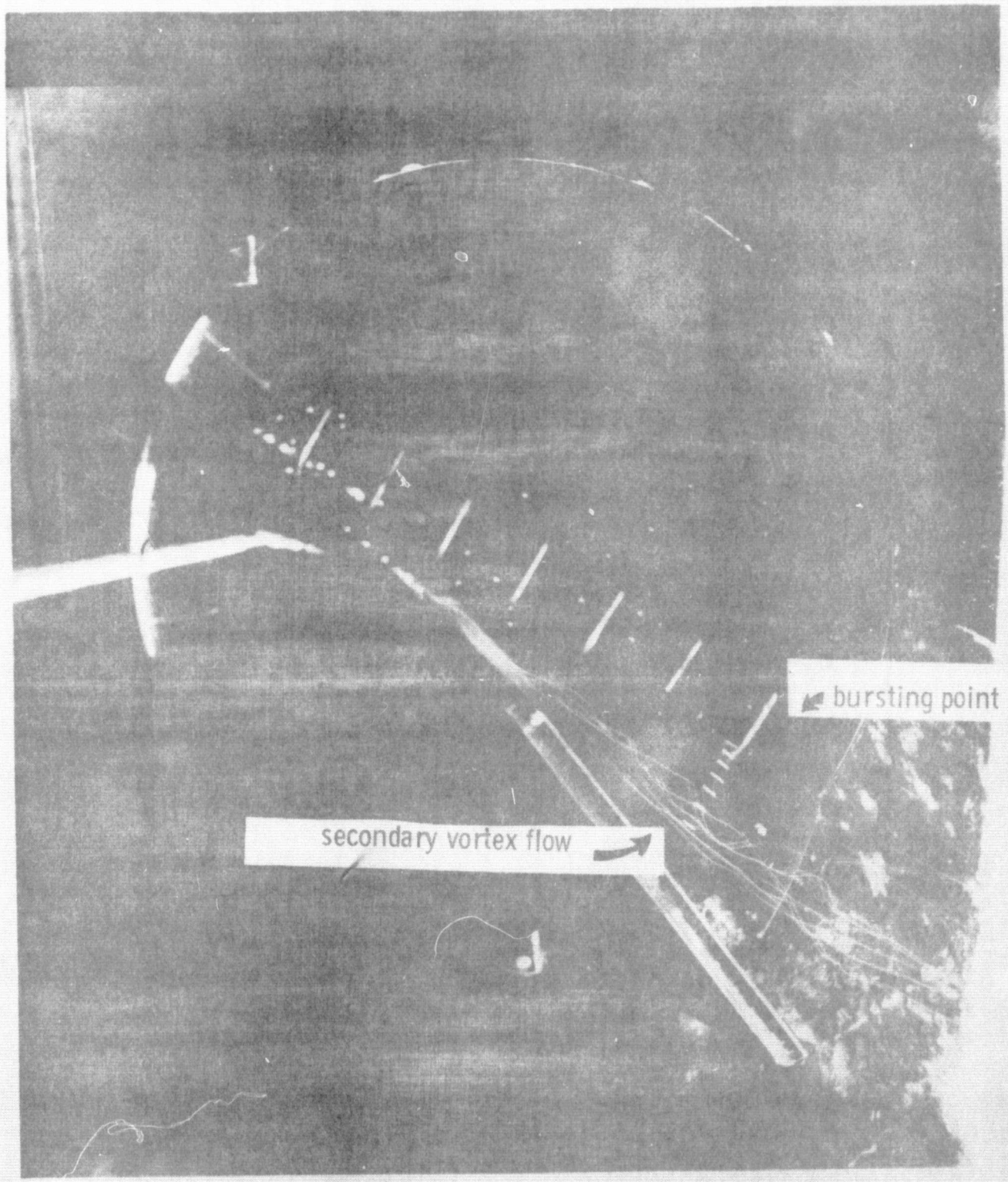

Figure 18. Secondary vortex and primary vortex bursting - Model III at 32^{0} angle of attack

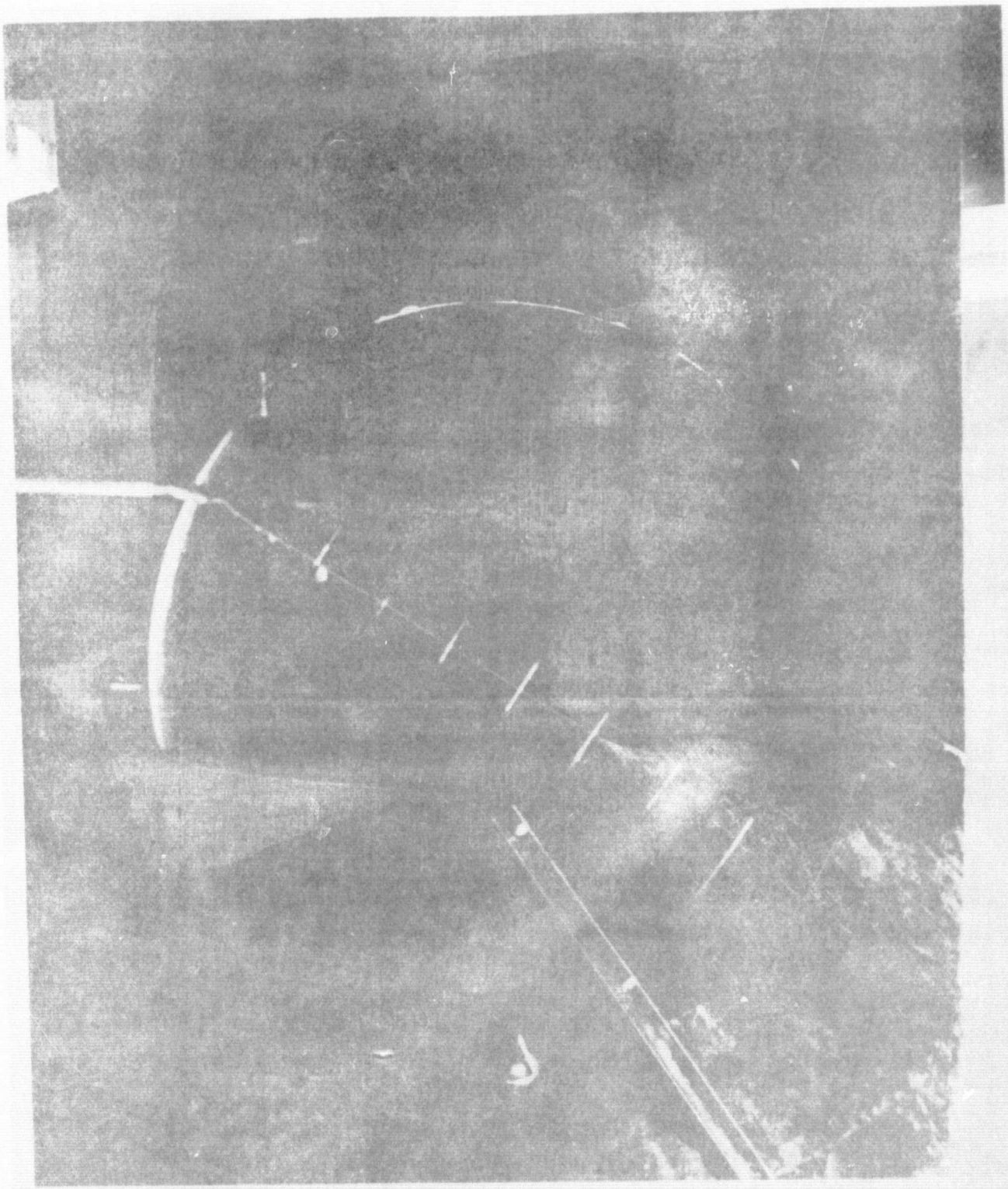

Figure 19. Primary vortex bursting for Model I at 35° angle of attack

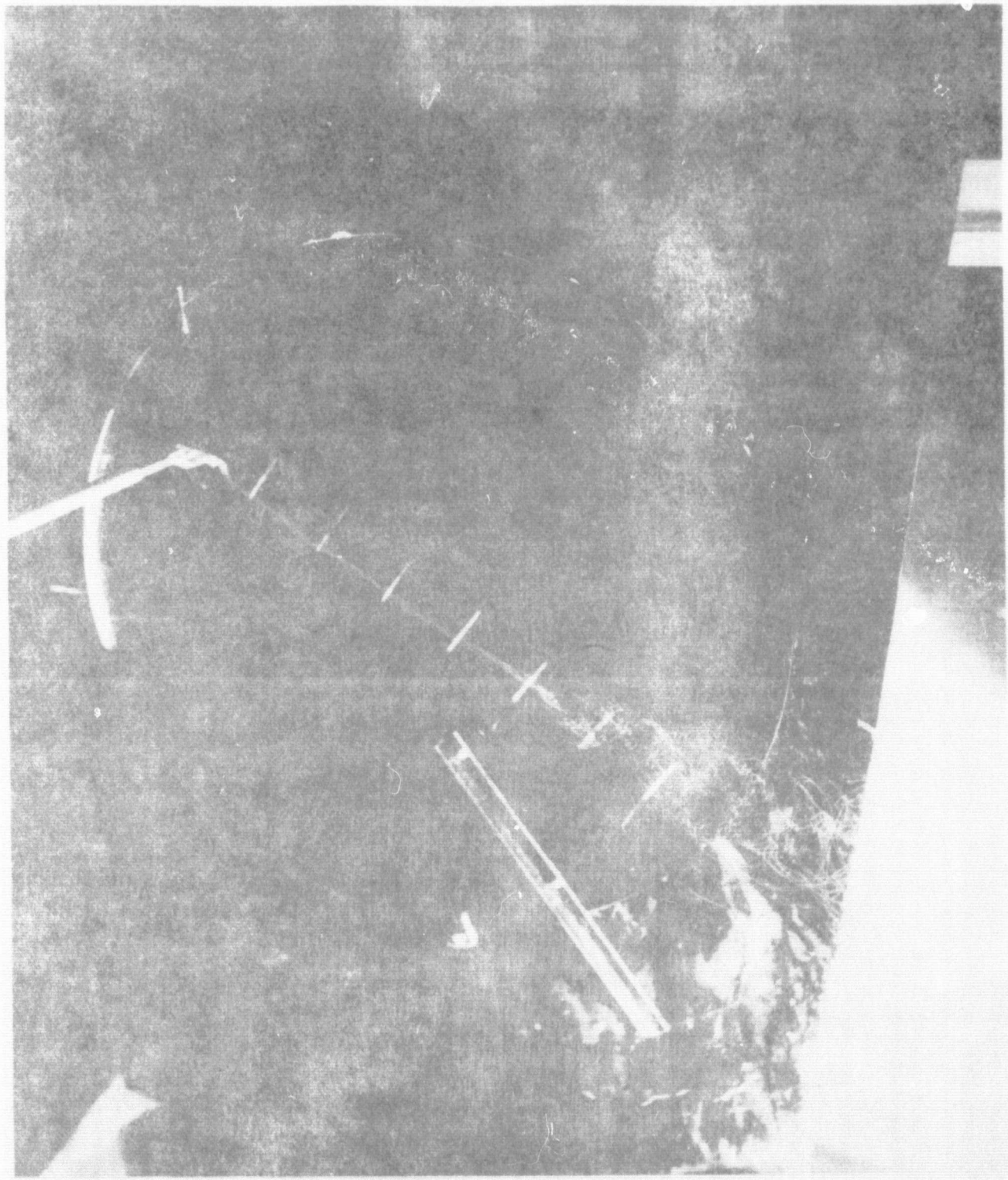

Figure 20. Primary vortex bursting for Model II at 35^{0} angle of attack

Figure 21. Primary vortex bursting for Model III at 35^{0} angle of attack

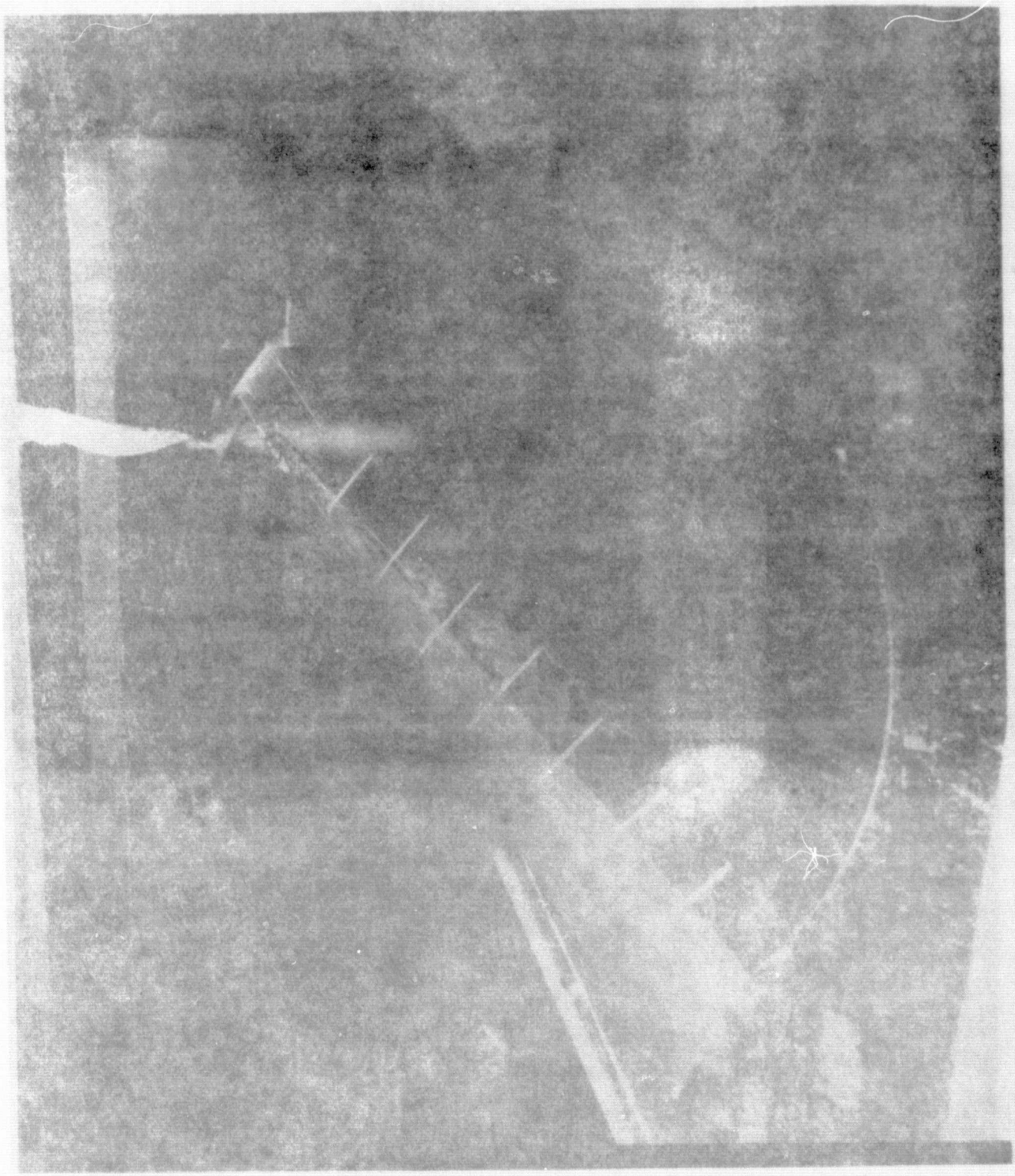

Figure 22. Primary vortex bursting for Model I at 40° angle of attack

Figure 23. Primary vortex bursting for Model II at 40° angle of attack

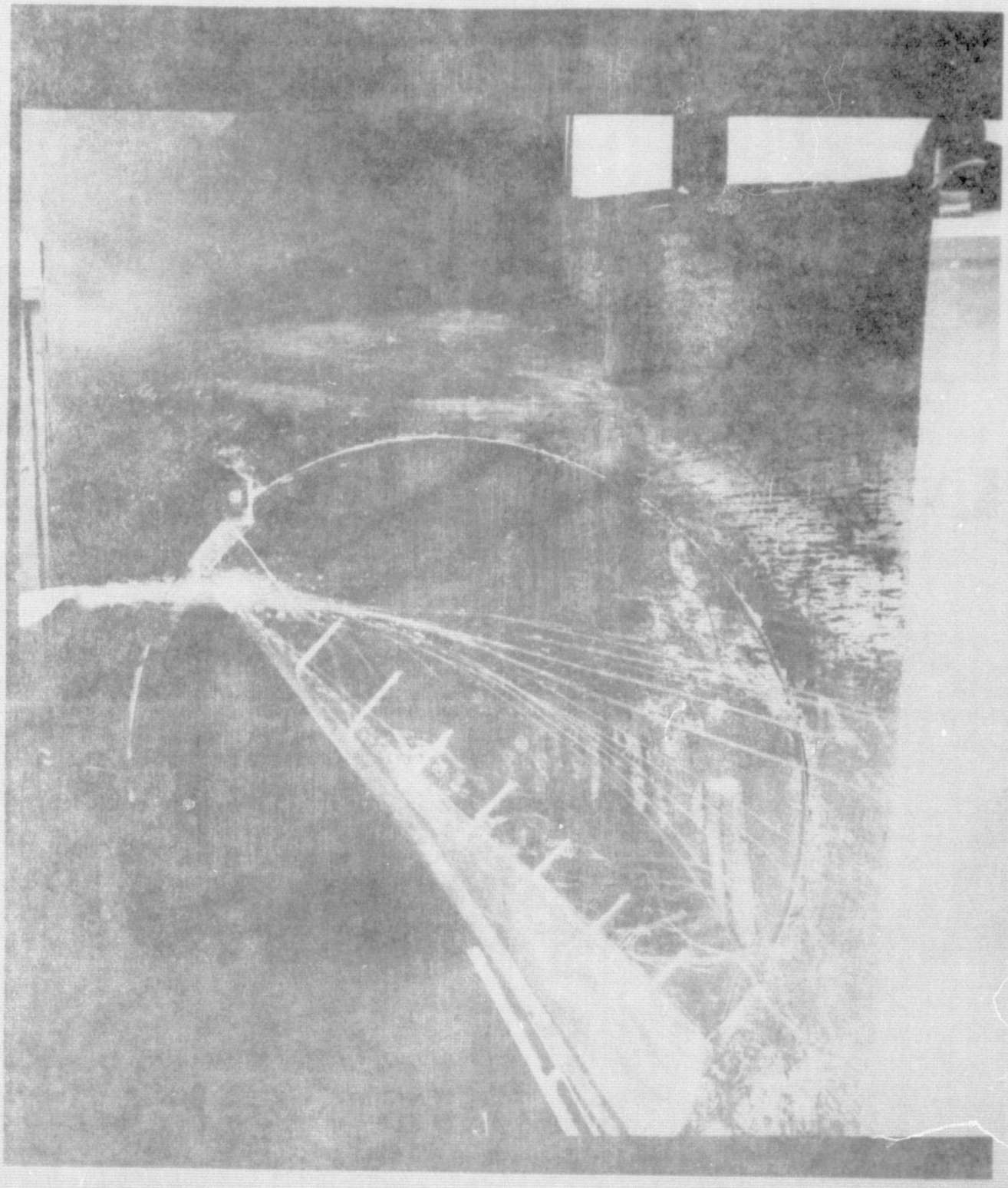

Figure 24. Primary vortex bursting for Model 111 at 40° angle of attack

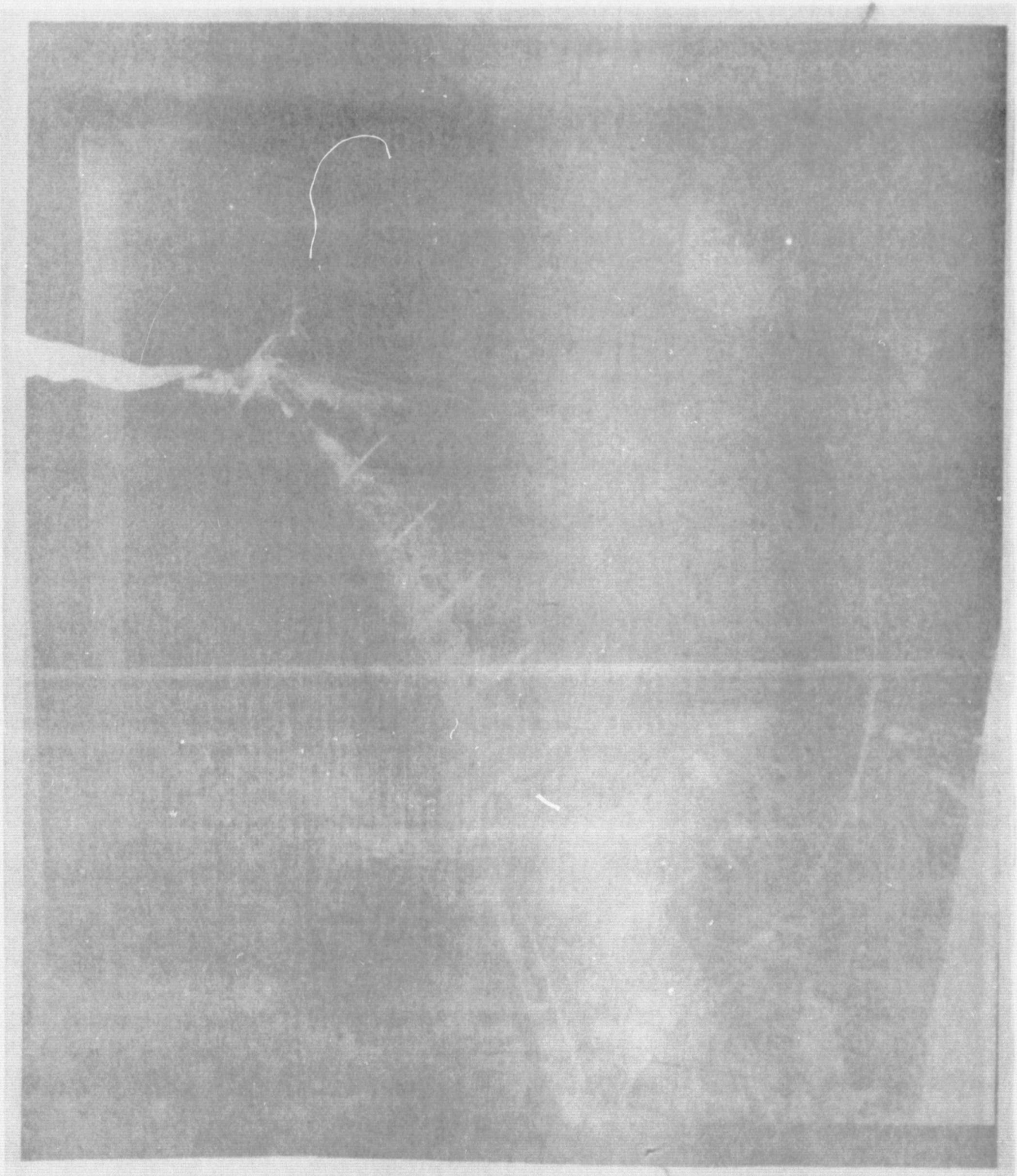

Figure 25. Bursting of primary vortex - Model I at 45° angle of attack

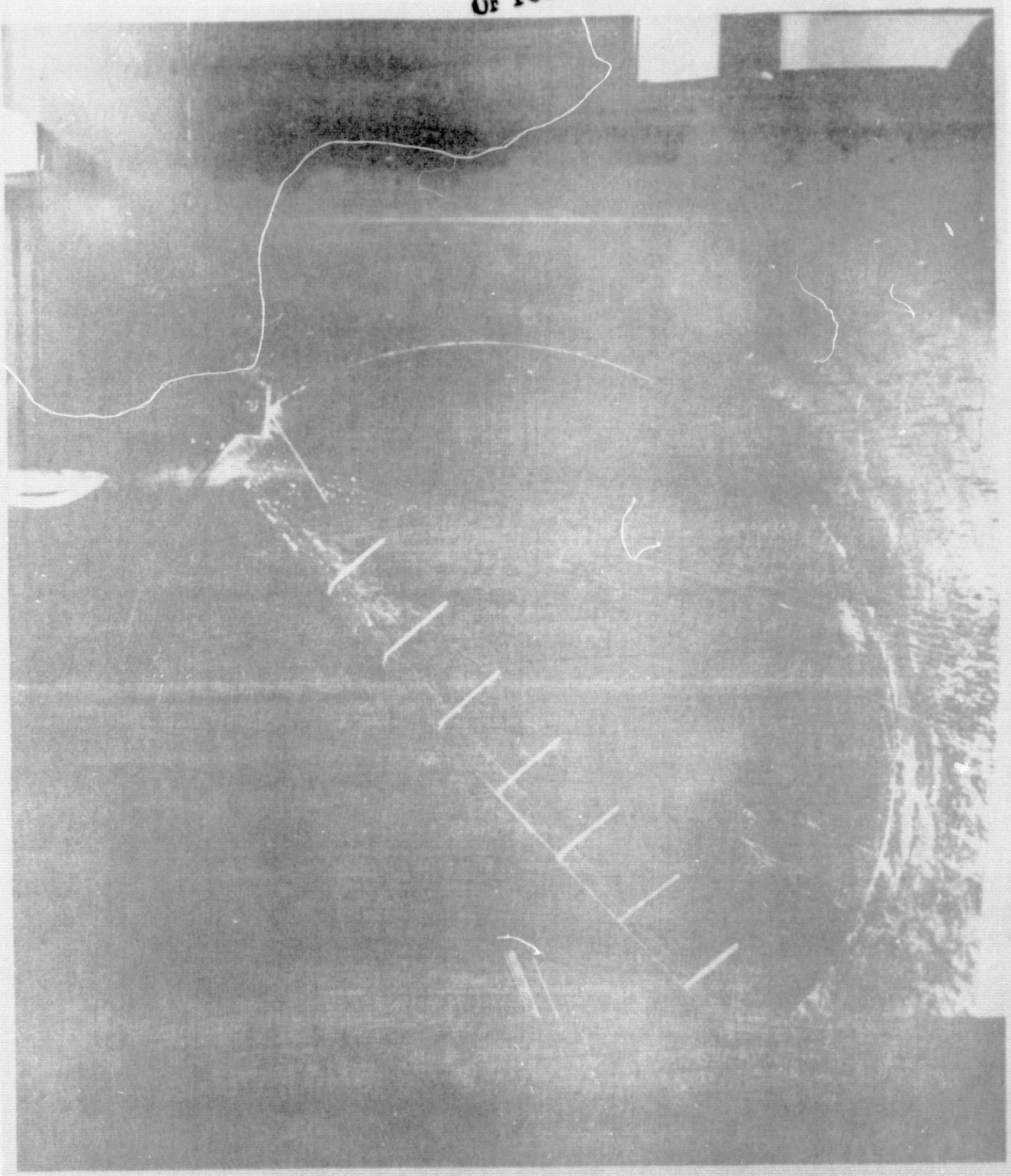

Figure 26. Bursting of primary vortex - Model II at 45^{0} angle of attack

Figure 27. Bursting of primary vortex - Model III at 45^{0} angle of attack

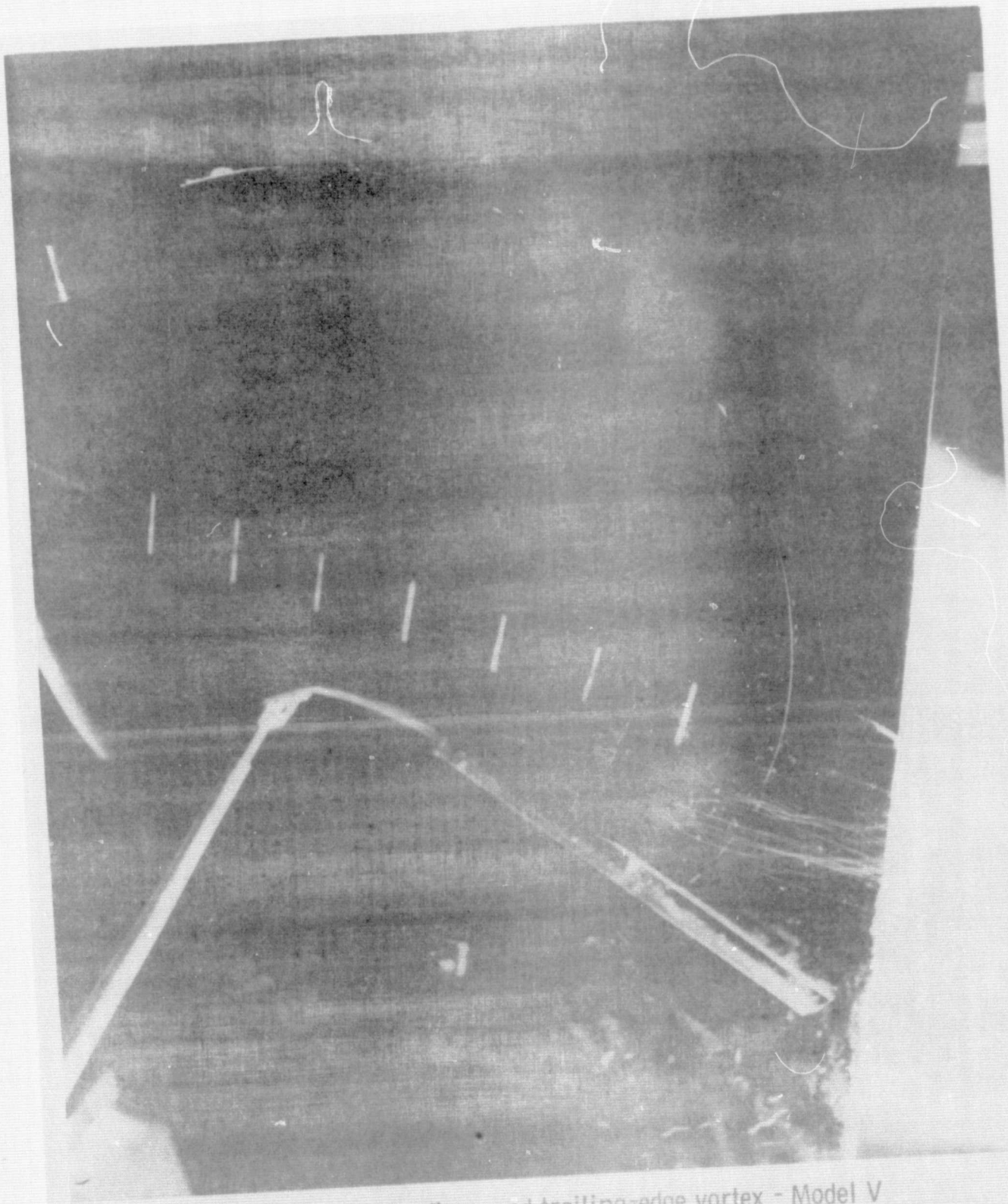

Figure 28. Leading- and trailing-edge vortex - Model V at 15° angle of attack

Figure 29. Leading-edge vortex - Model IV at 15° angle of attack

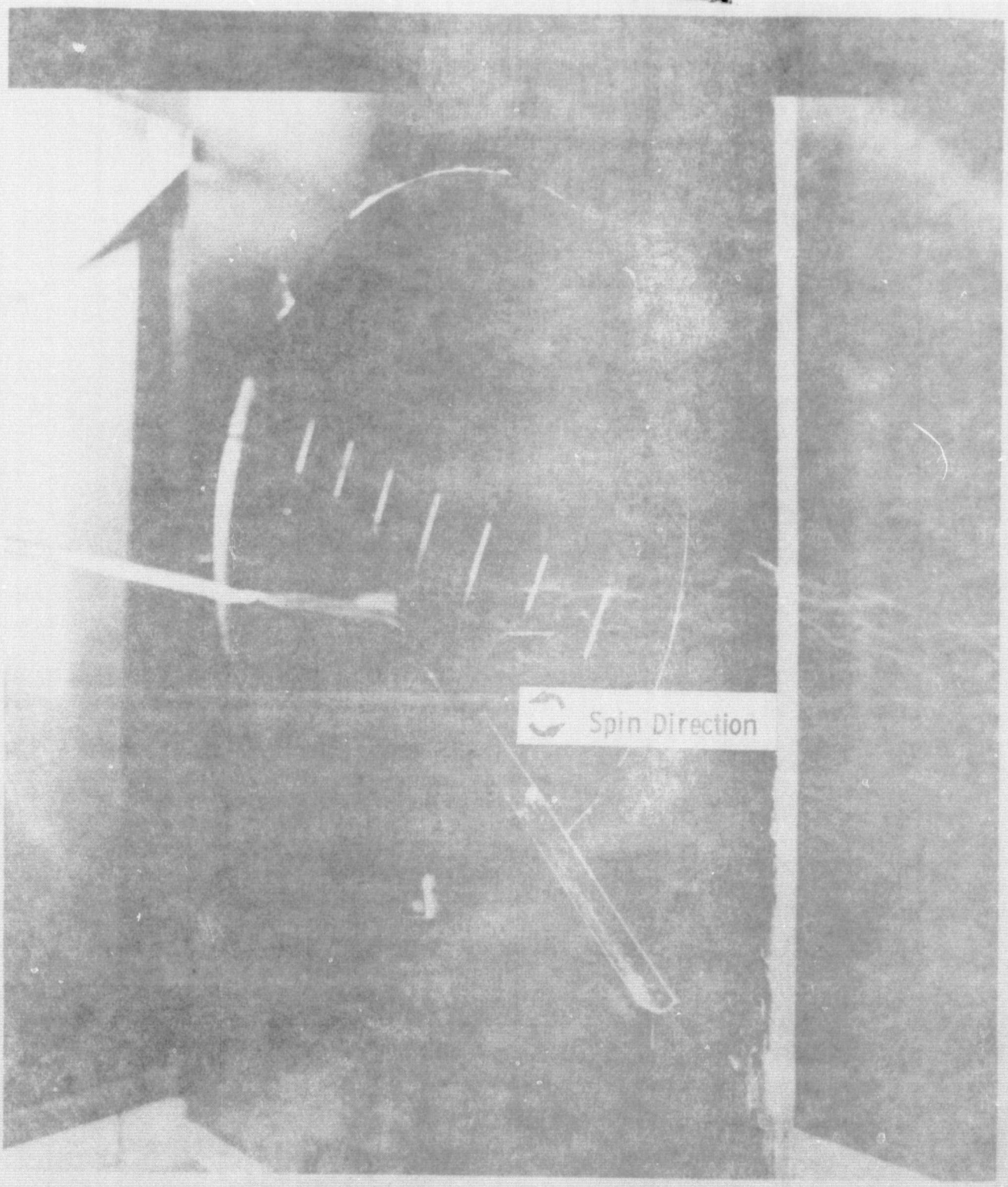

Figure 30. Spin direction of trailing-edge vortex - Model IV at 25° angle of attack

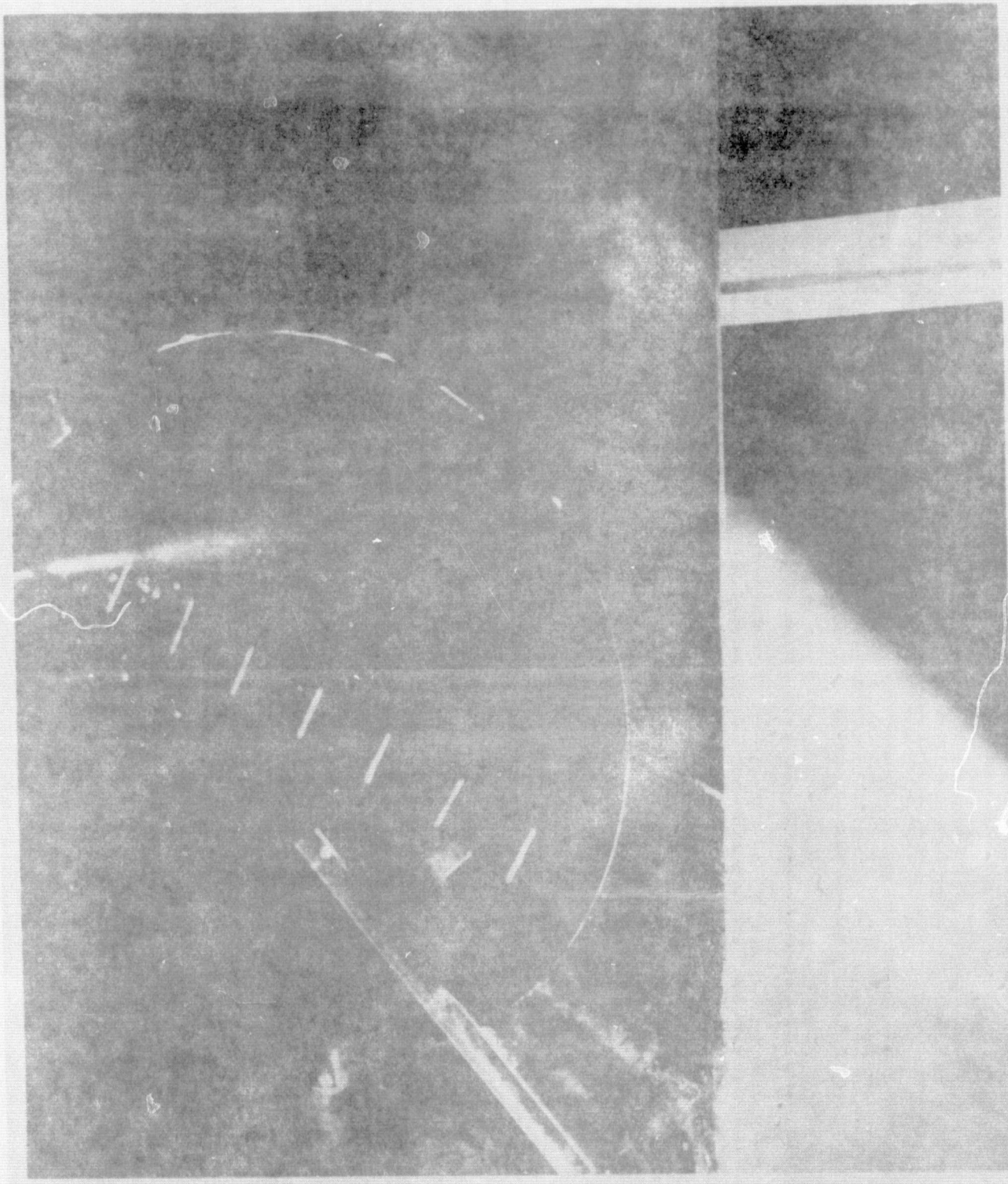

Figure 31. Primary vortex core of Model IV at 30° angle of attack

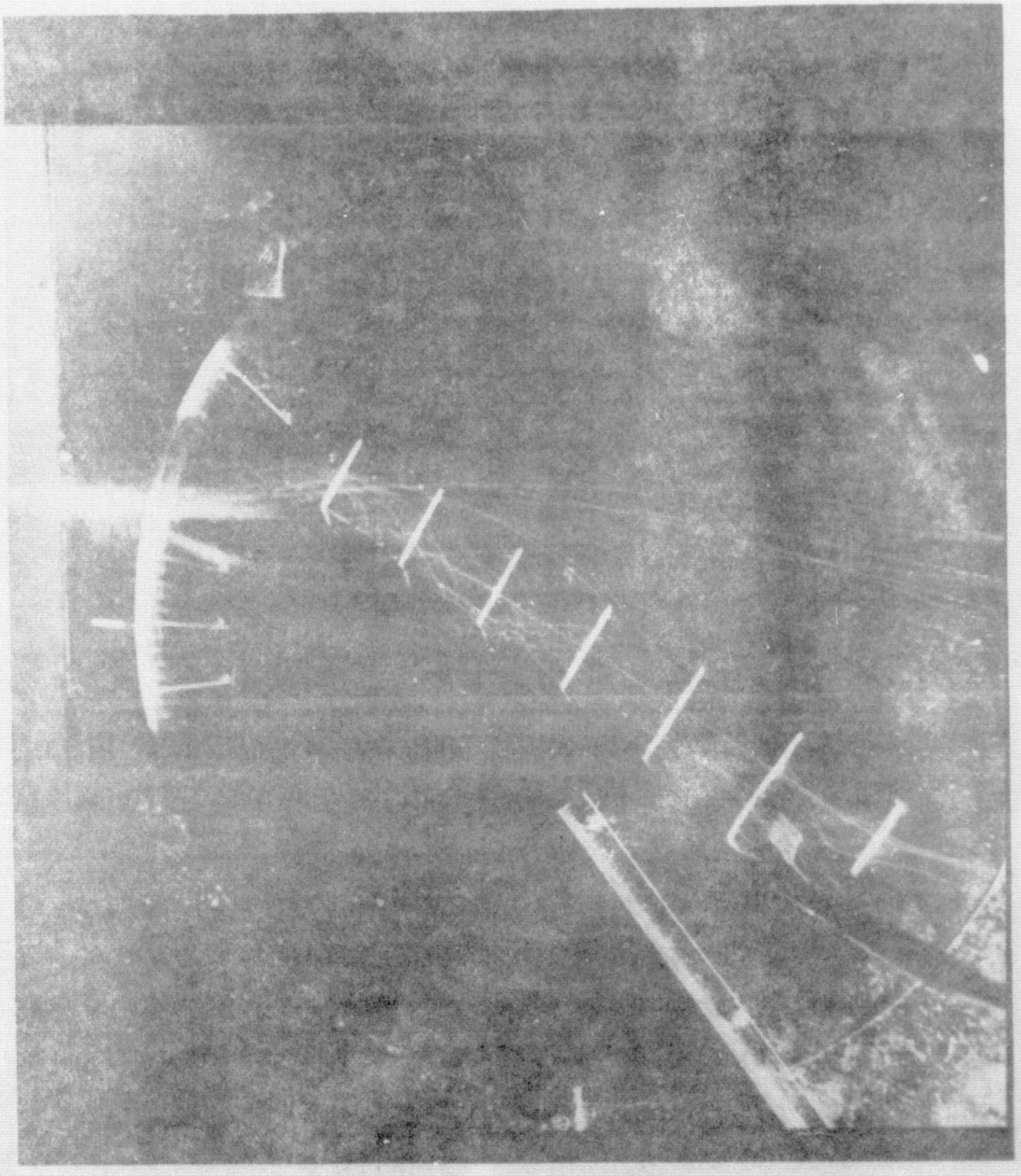

Figure 32. Primary vortex core of Model V at 30^{0} angle of attack

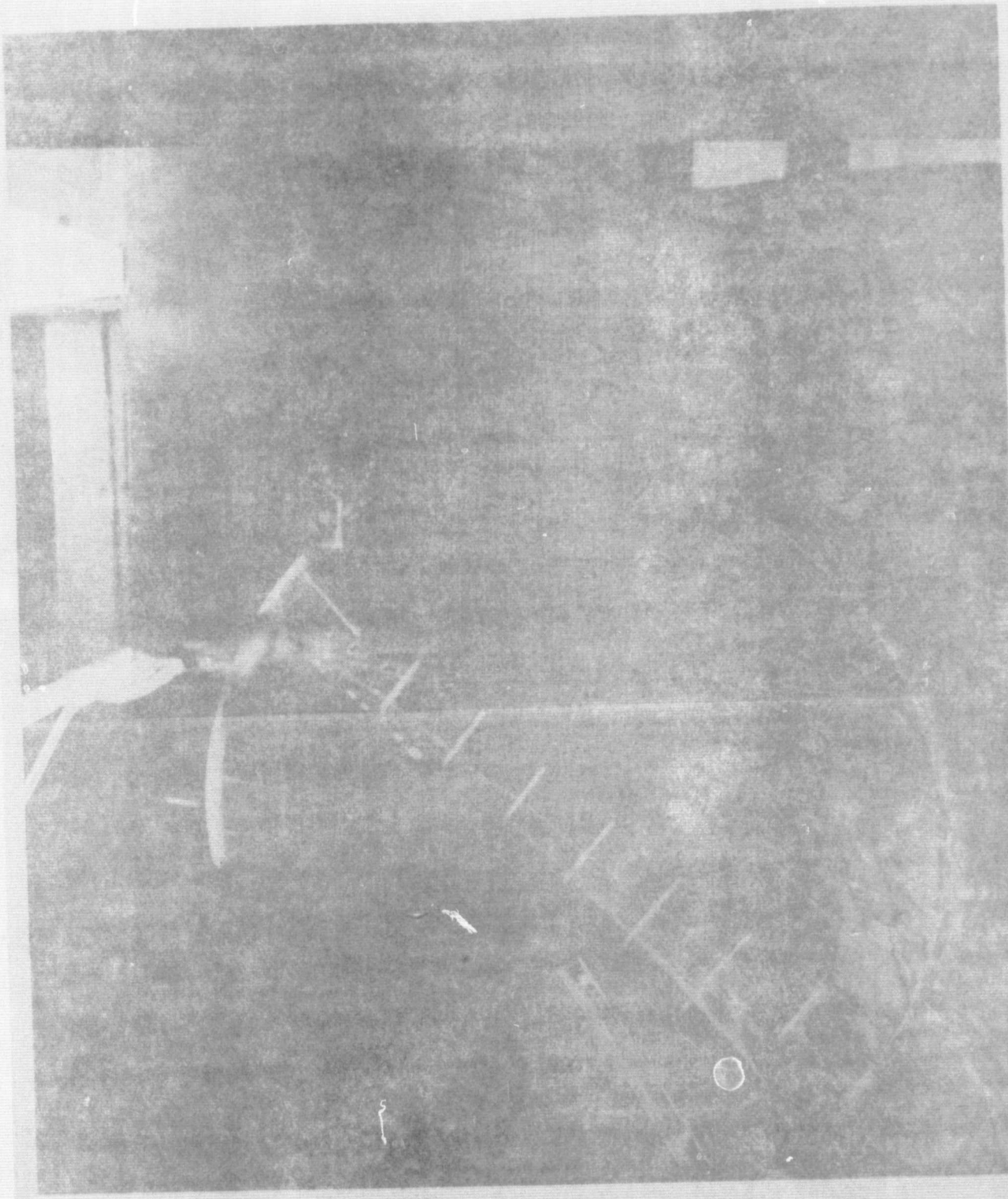

Figure 33. Bursting point at trailing edge - Model IV at 35° angle of attack

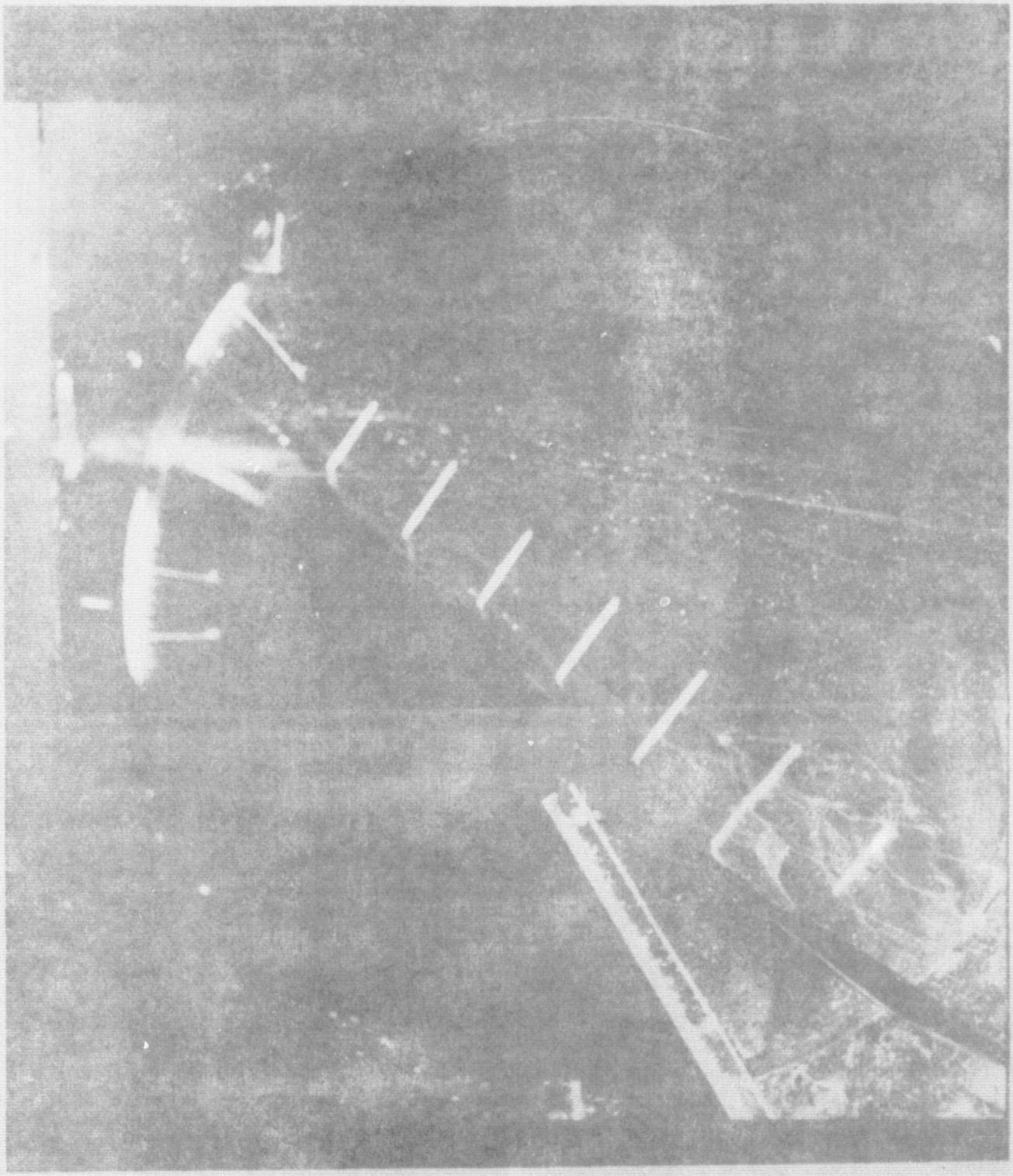

Figure 34. Bursting point at trailing-edge - Model V at 35^0 angle of attack

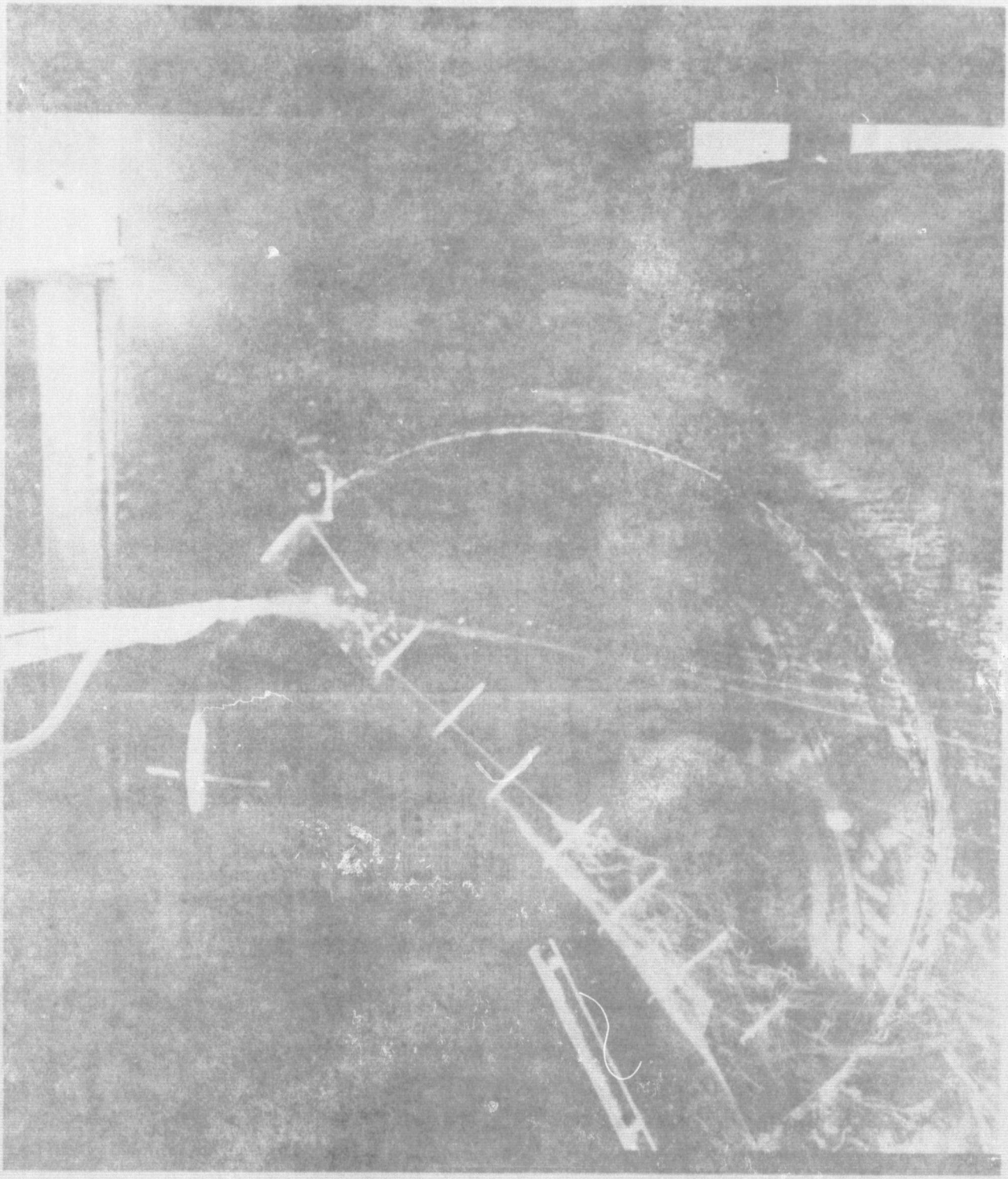

Figure 35. Primary vortex bursting - Model IV at 40° angle of attack

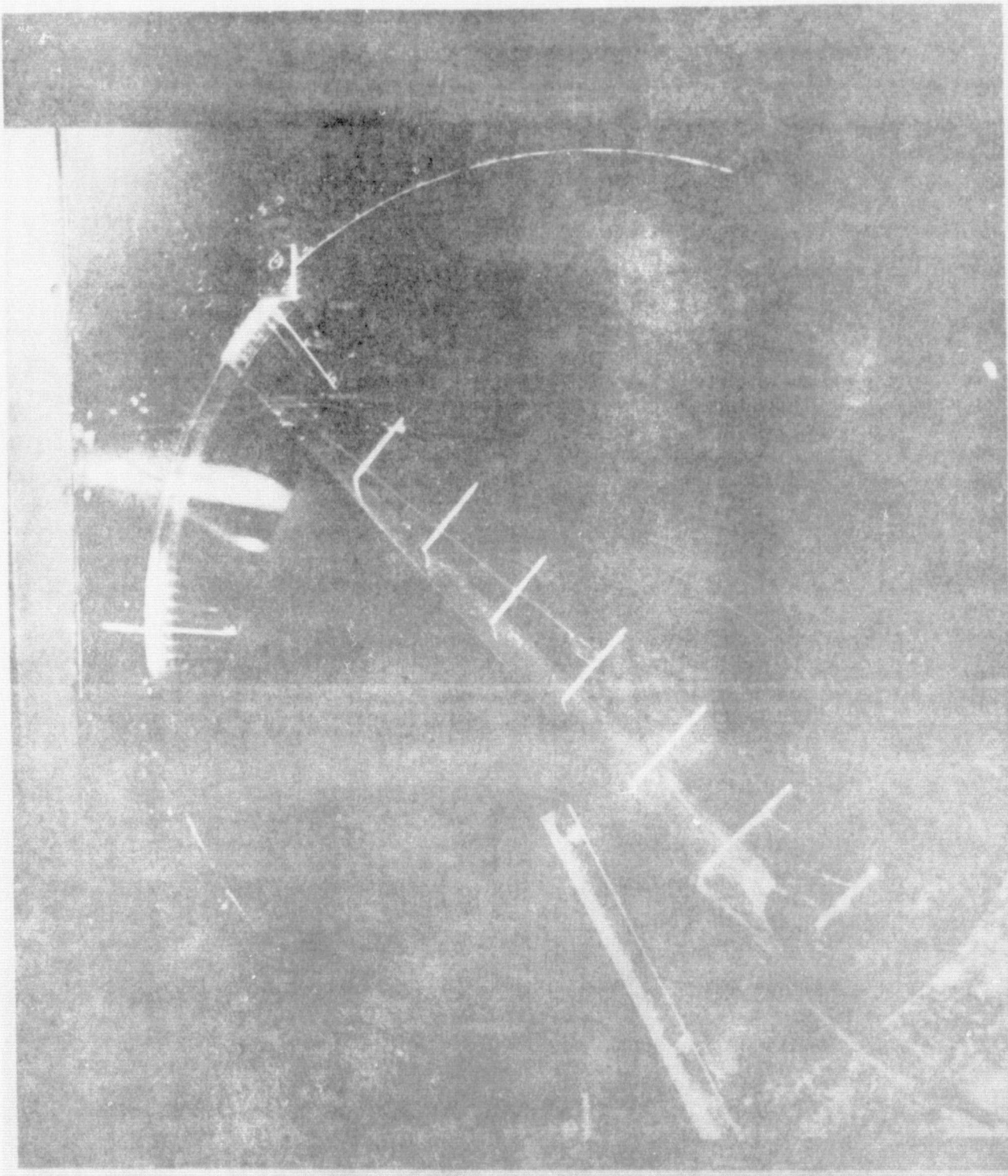

Figure 36. Primary vortex bursting - Model V at 40° angle of attack

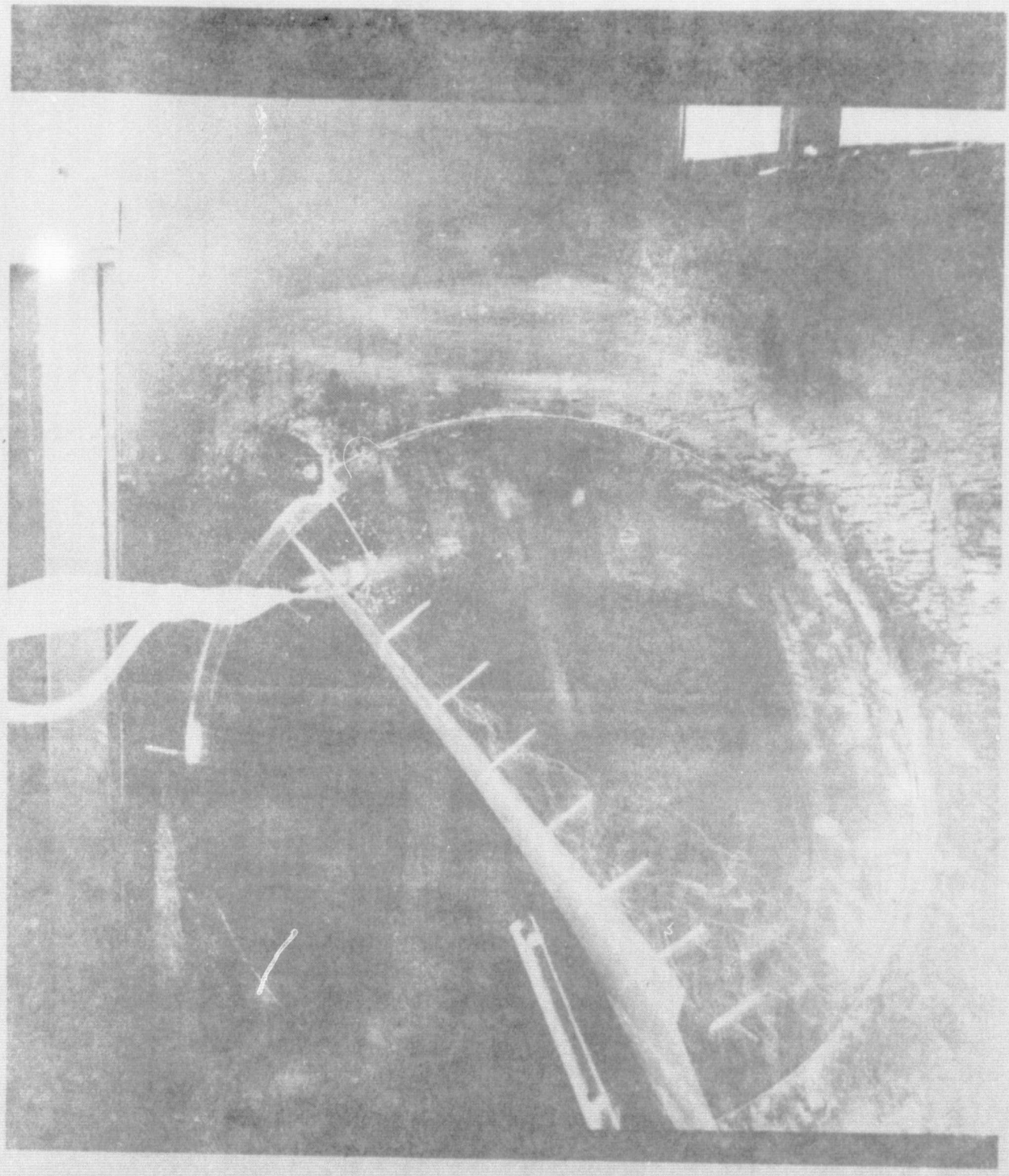

Figure 37. Primary vortex bursting - Model IV at 45° angle of attack

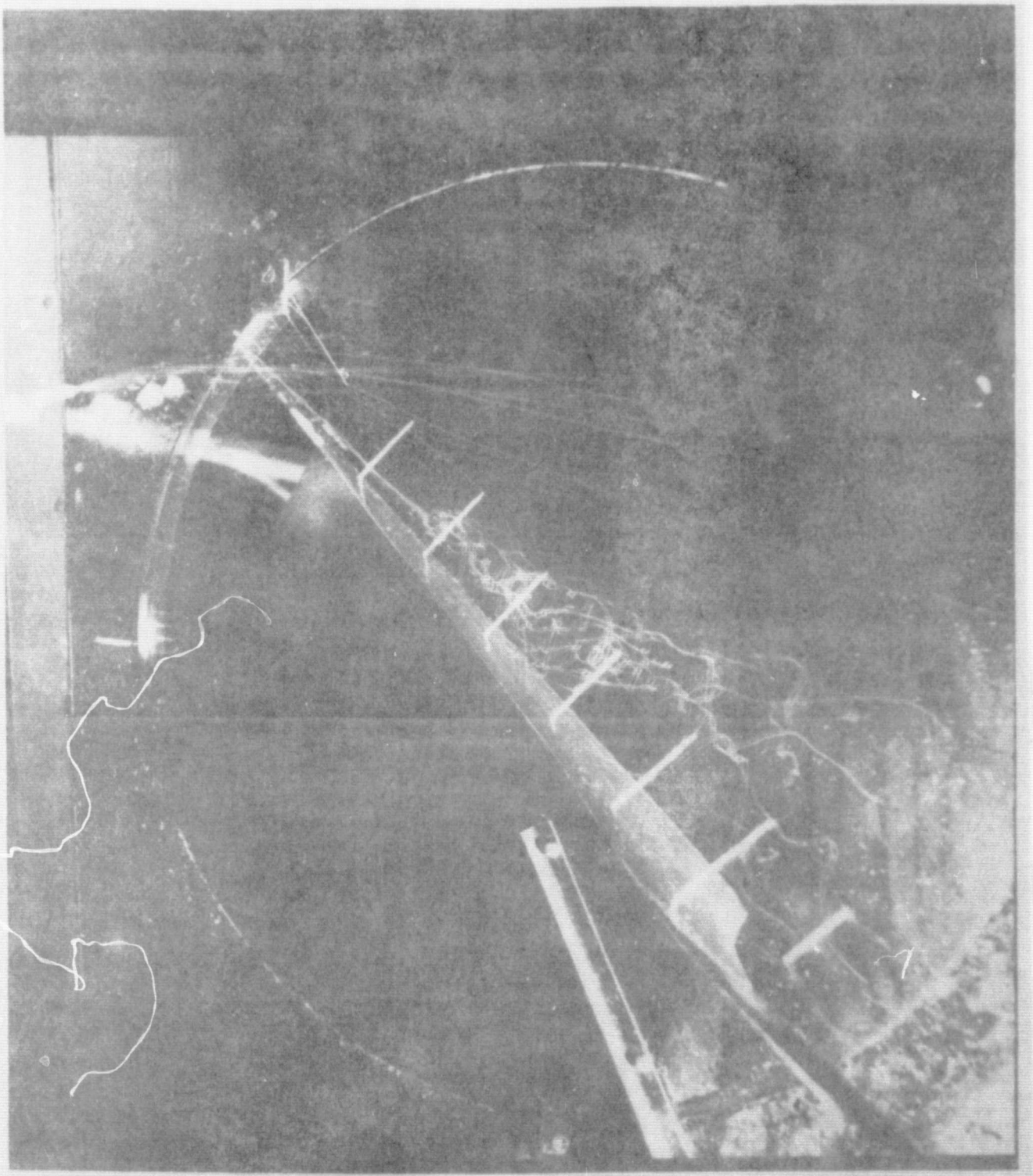

Figure 38. Primary vortex bursting - Model V at 45° angle of attack

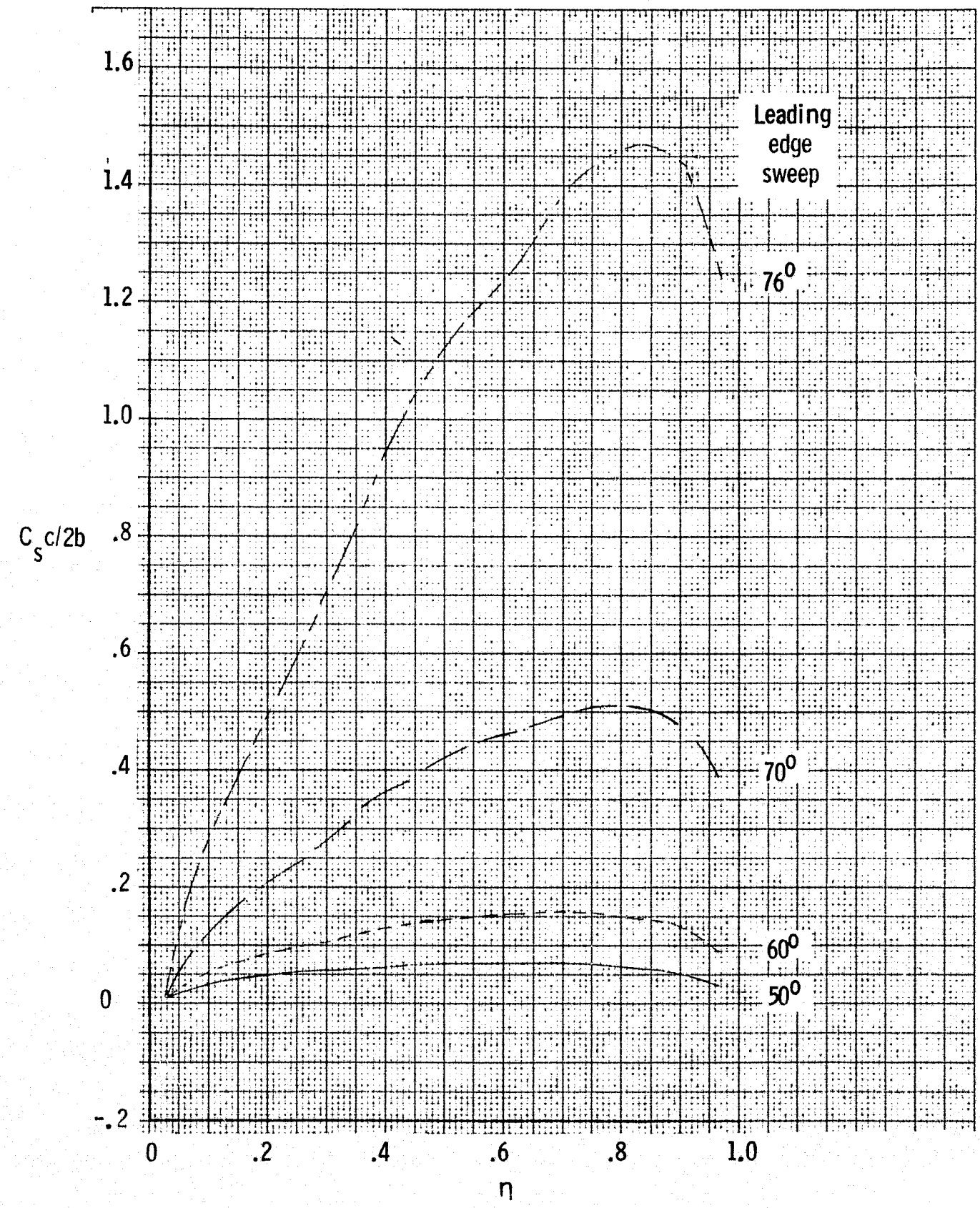

Figure 39. Section suction distribution for four delta wings.

EQUATION OF LEADING EDGE

WING 2E: $y_2 = .2331 + .4663(X - .5) - .496 (X - .5)^{2.278}$; FOR $X > .5$

WING 4E: $y_4 = .781\ y_2$

WING 5E: $y_5 = -11 X^6 + 48.5224 X^5 - 85.1382 X^4 + 74.7491 X^3$

$- 34.2379 X^2 + 8.1672 X - .6989$; FOR $X > .35$

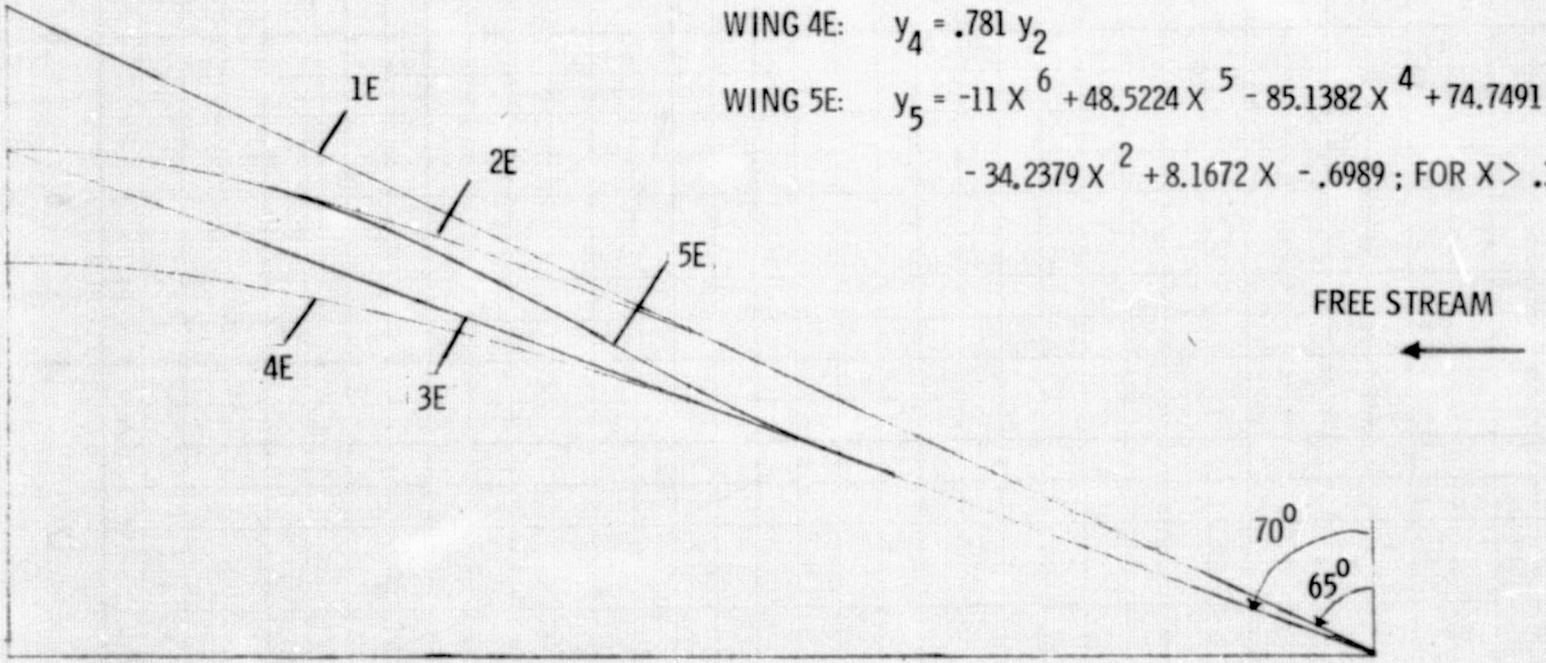

FIGURE 40. SEMI-SPAN PLANFORMS USED BY EARNSHAW.

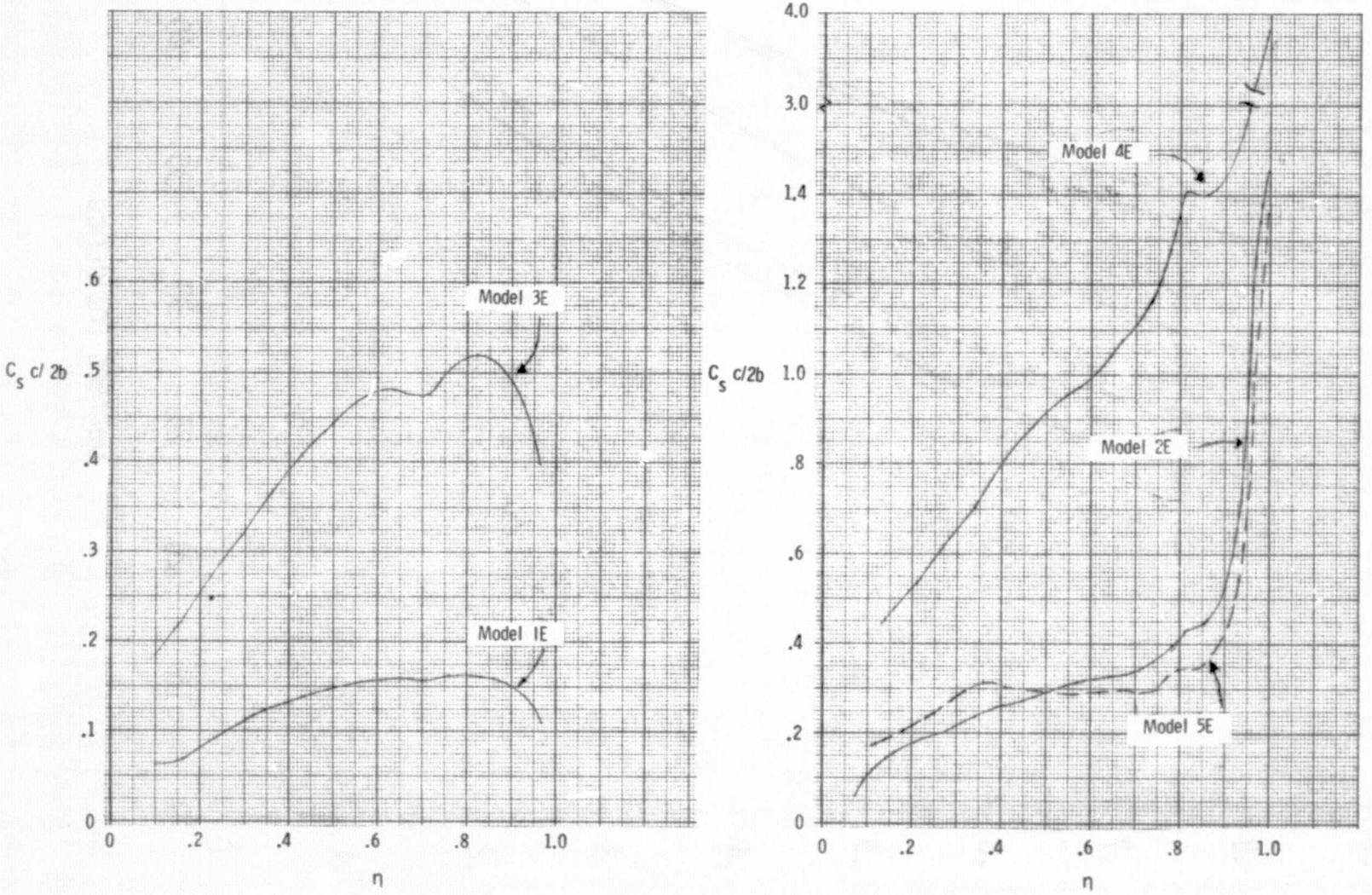

Figure 41. Section suction distribution for Earnshaw models.

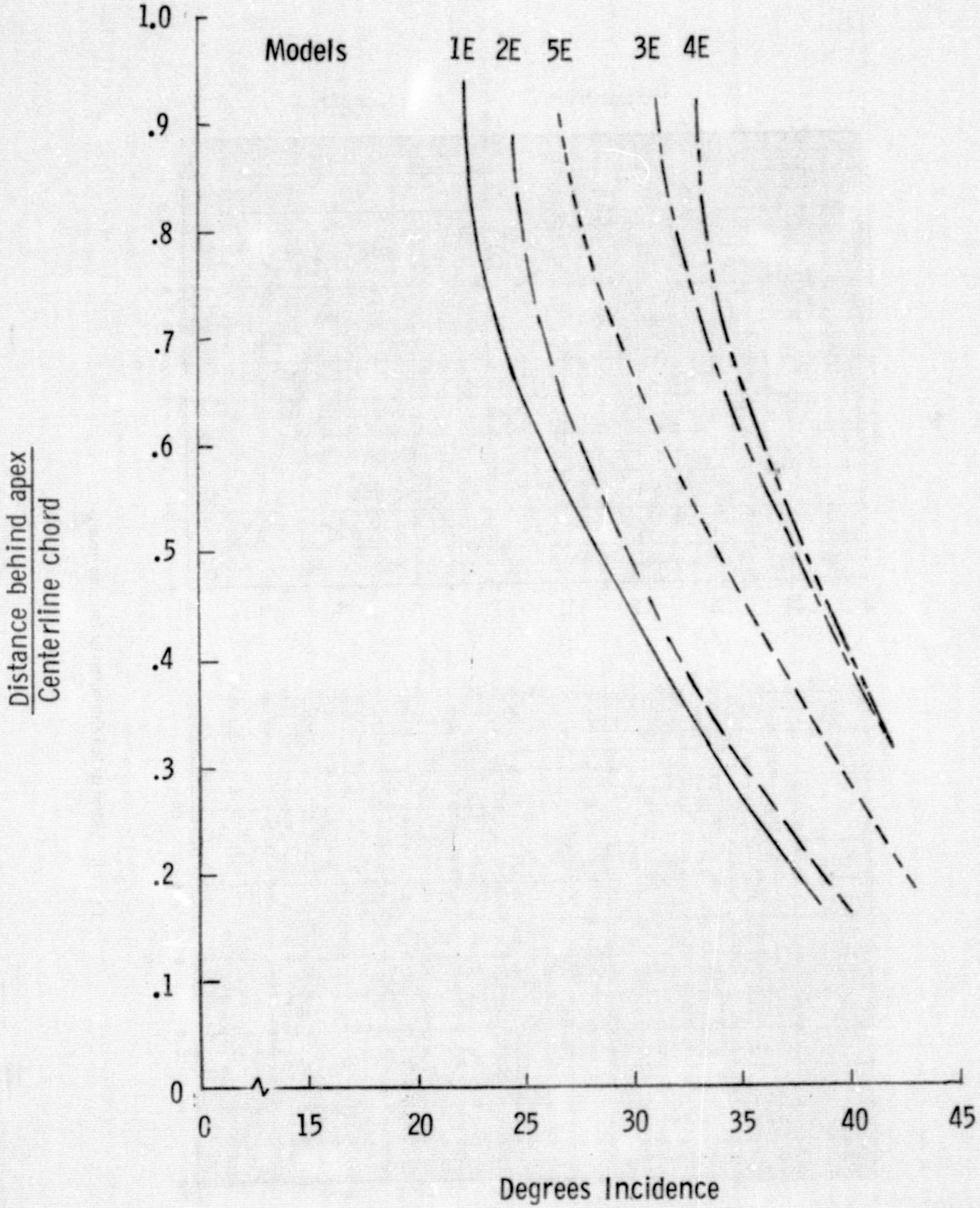

Figure 42. Earnshaw experimental results - variation of breakdown position.

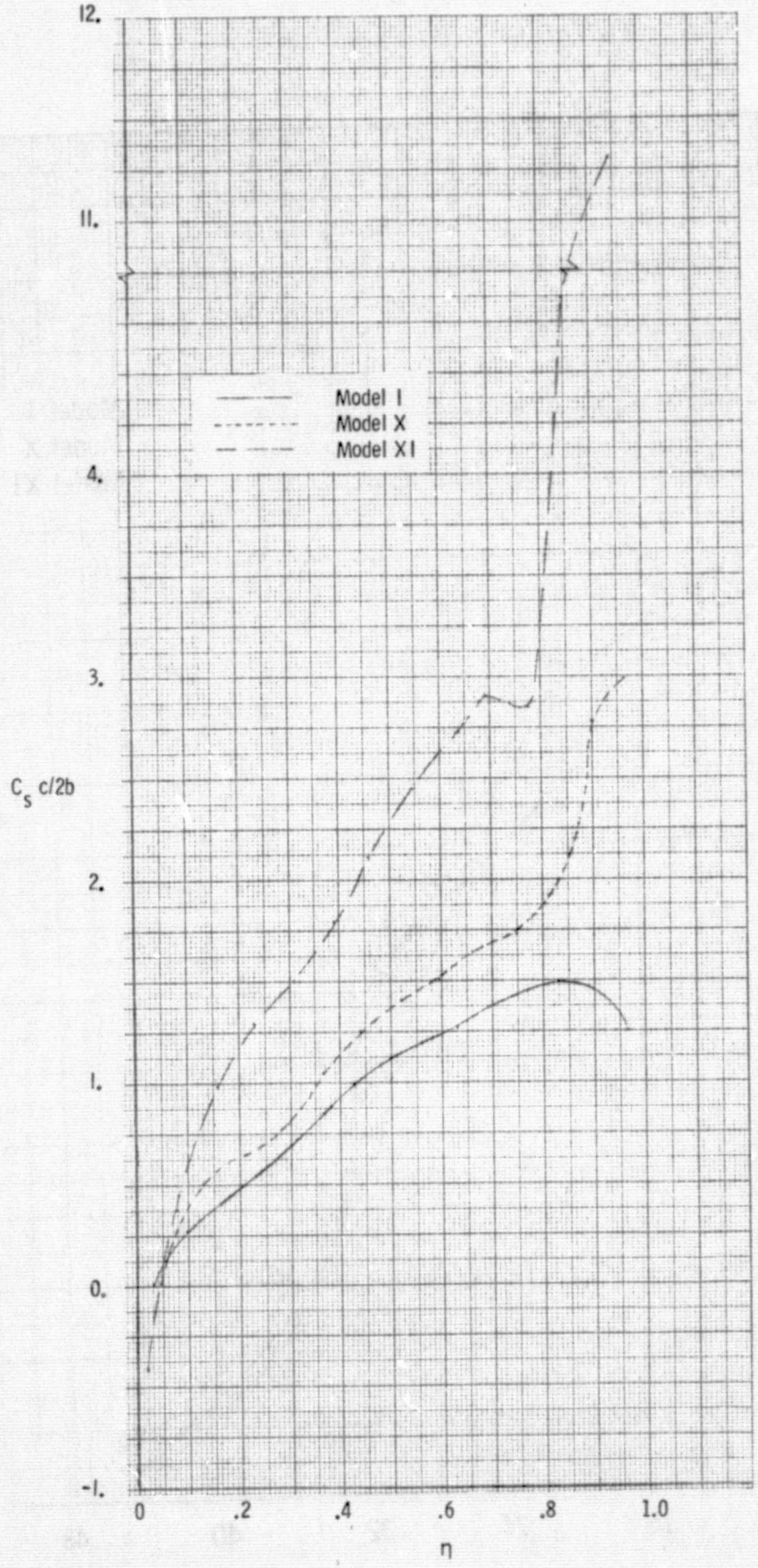

Figure 43. Section suction distribution - Models I, X, and XI.

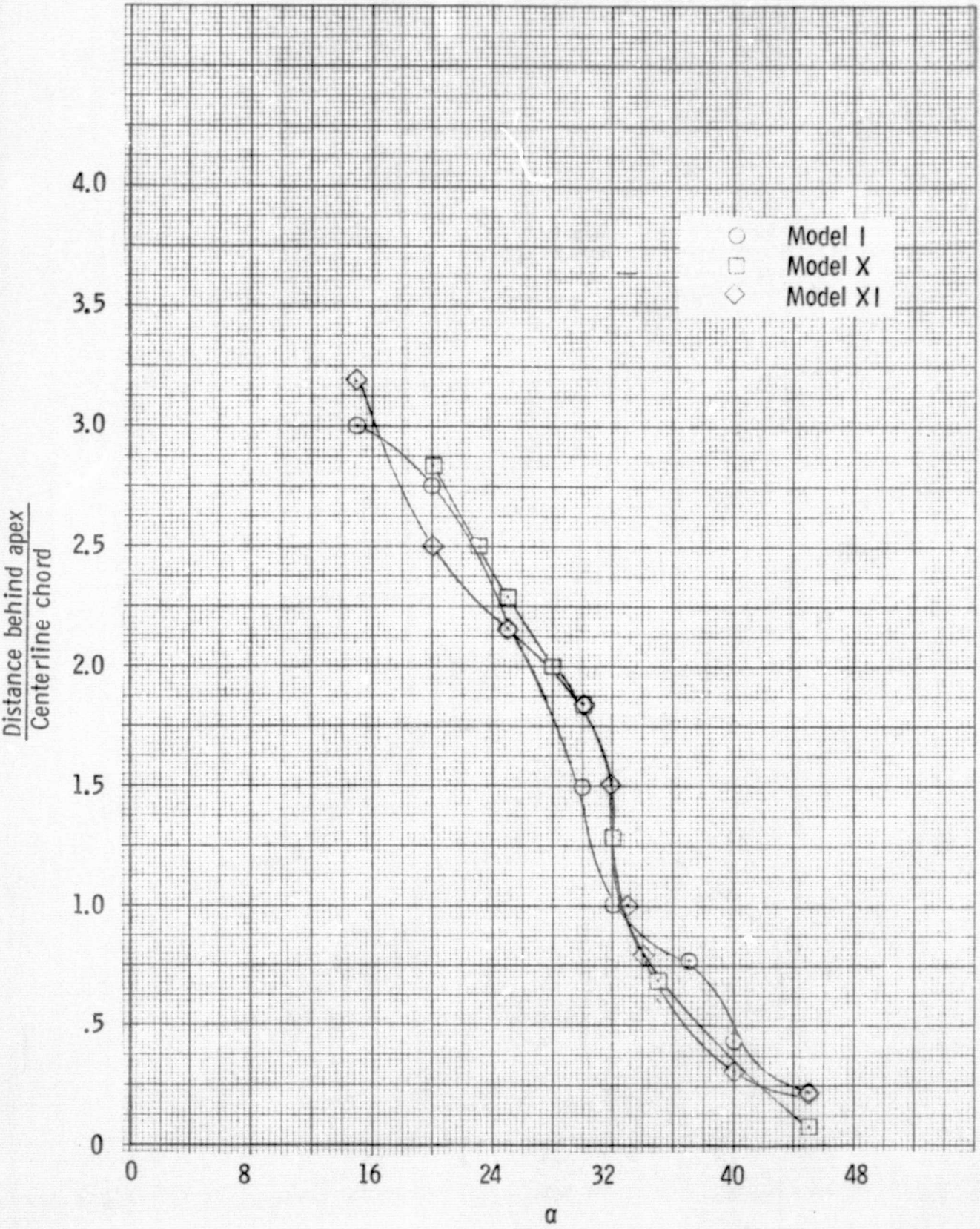

Figure 44. Vortex bursting position - Models I, X, and XI.

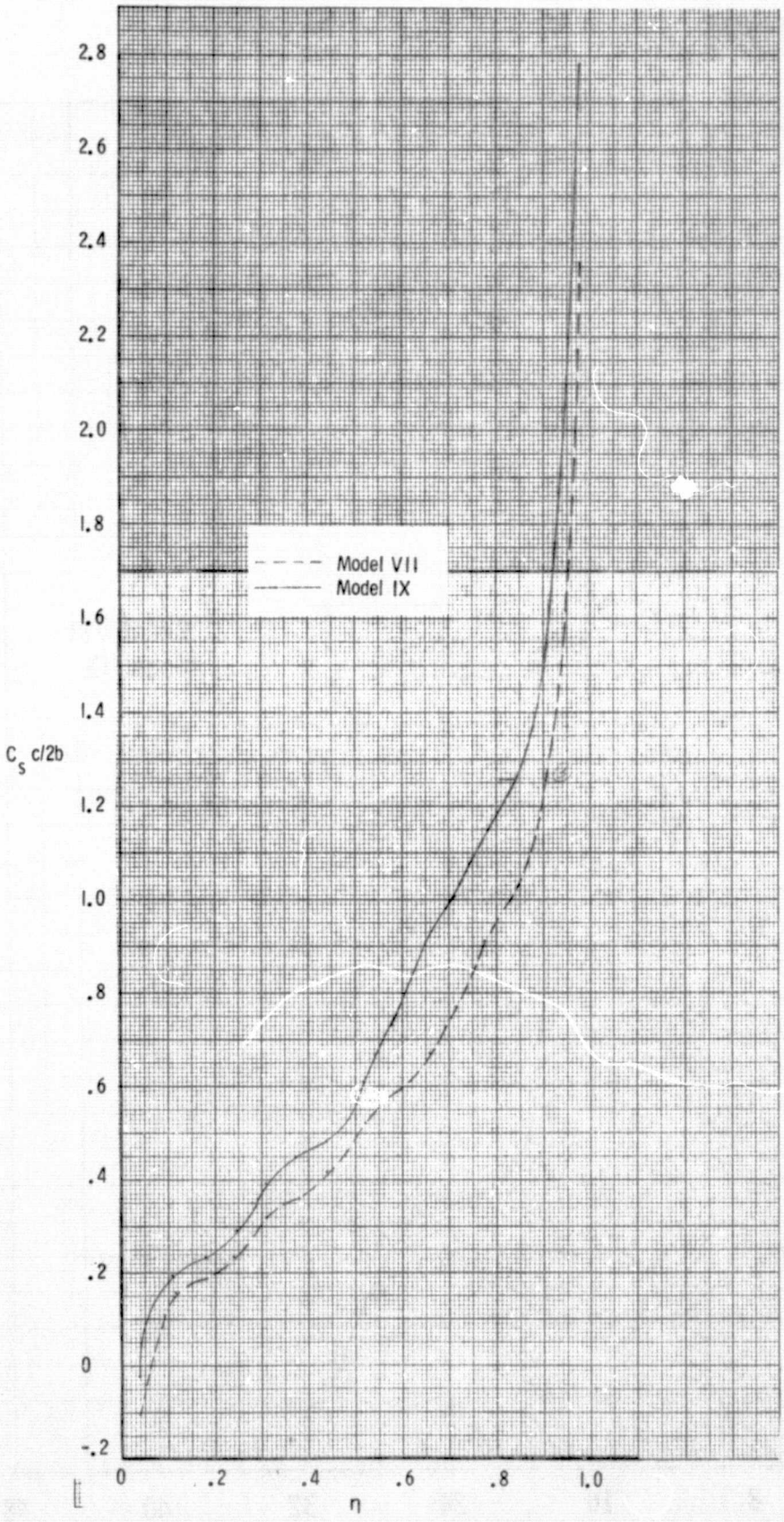

Figure 45. Section suction distribution - Models VII and IX.

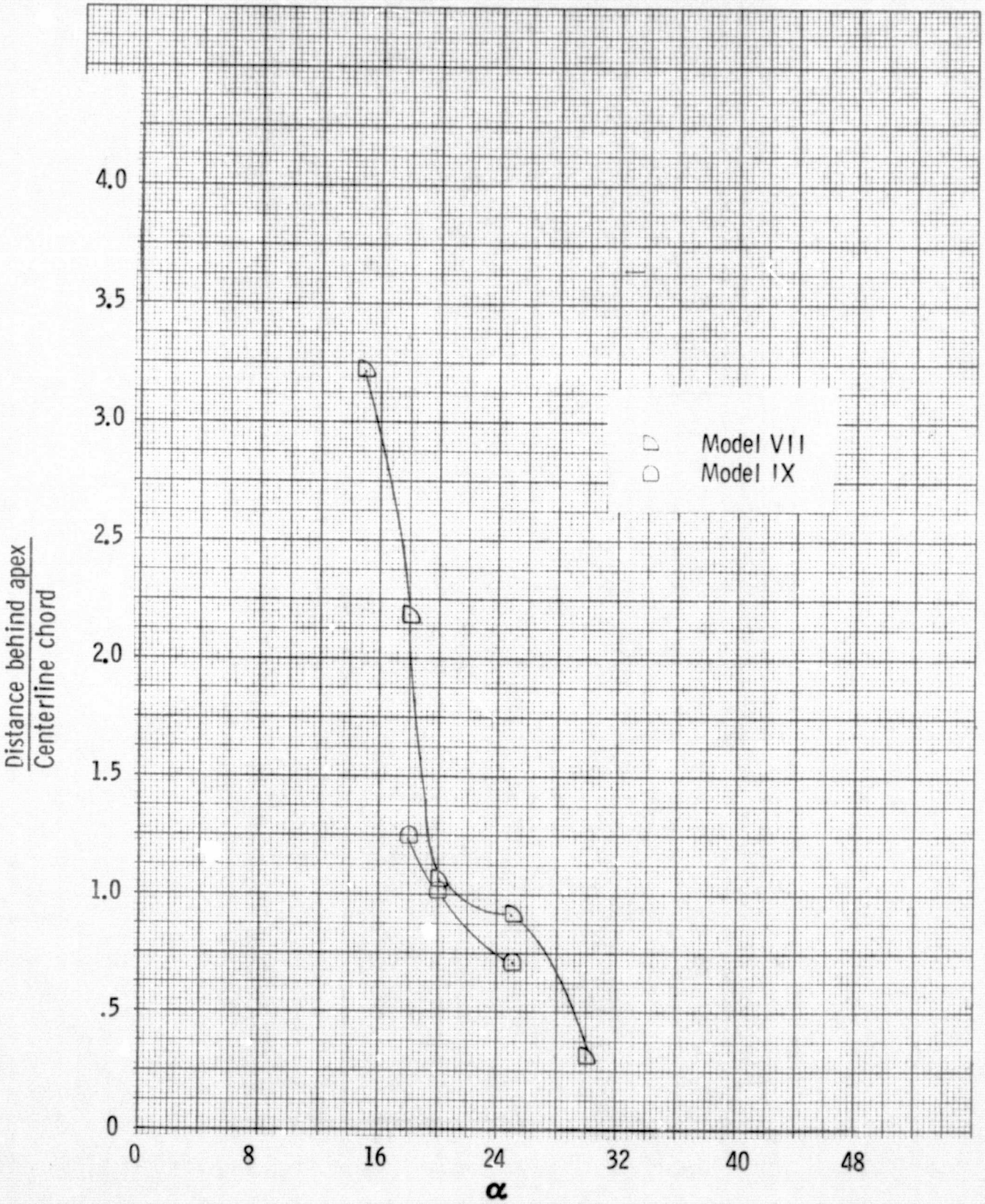

Figure 46. Vortex bursting position - Models VII and IX.

Figure 47. Model VII at 20 angle of attack.

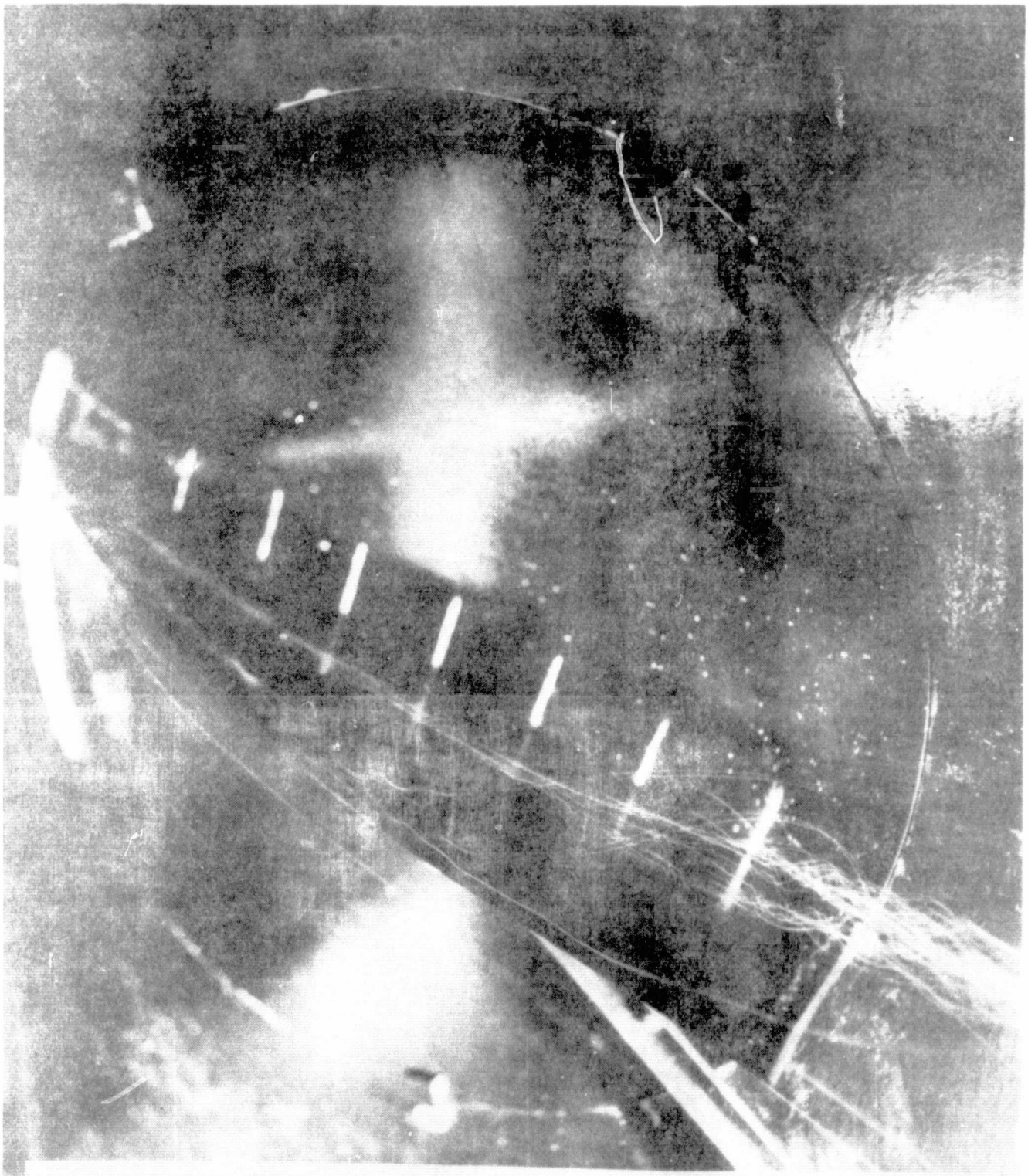

Figure 48. Model VII at 20° angle of attack with two bursting points.

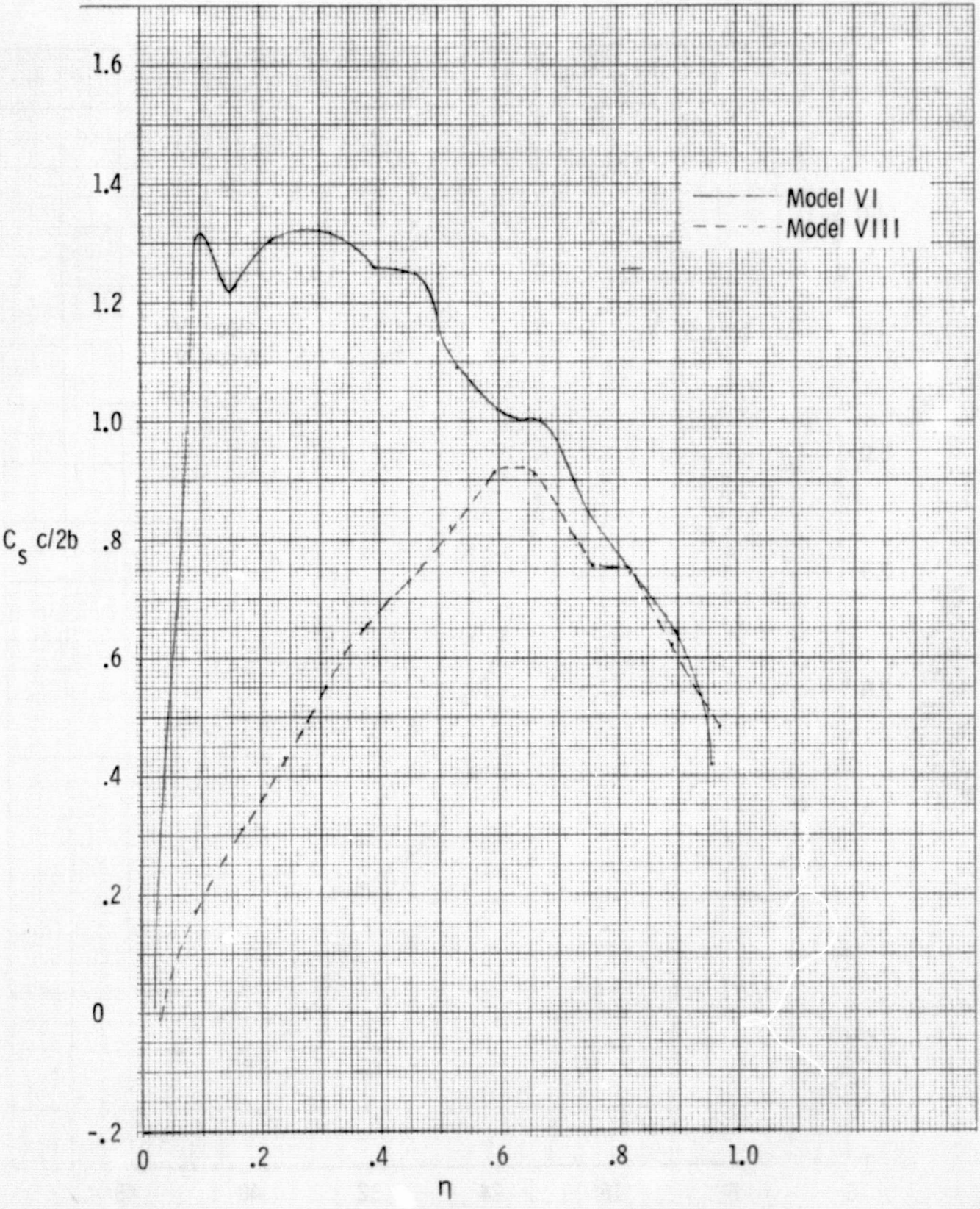

Figure 49. Section suction distribution - Models VI and VIII.

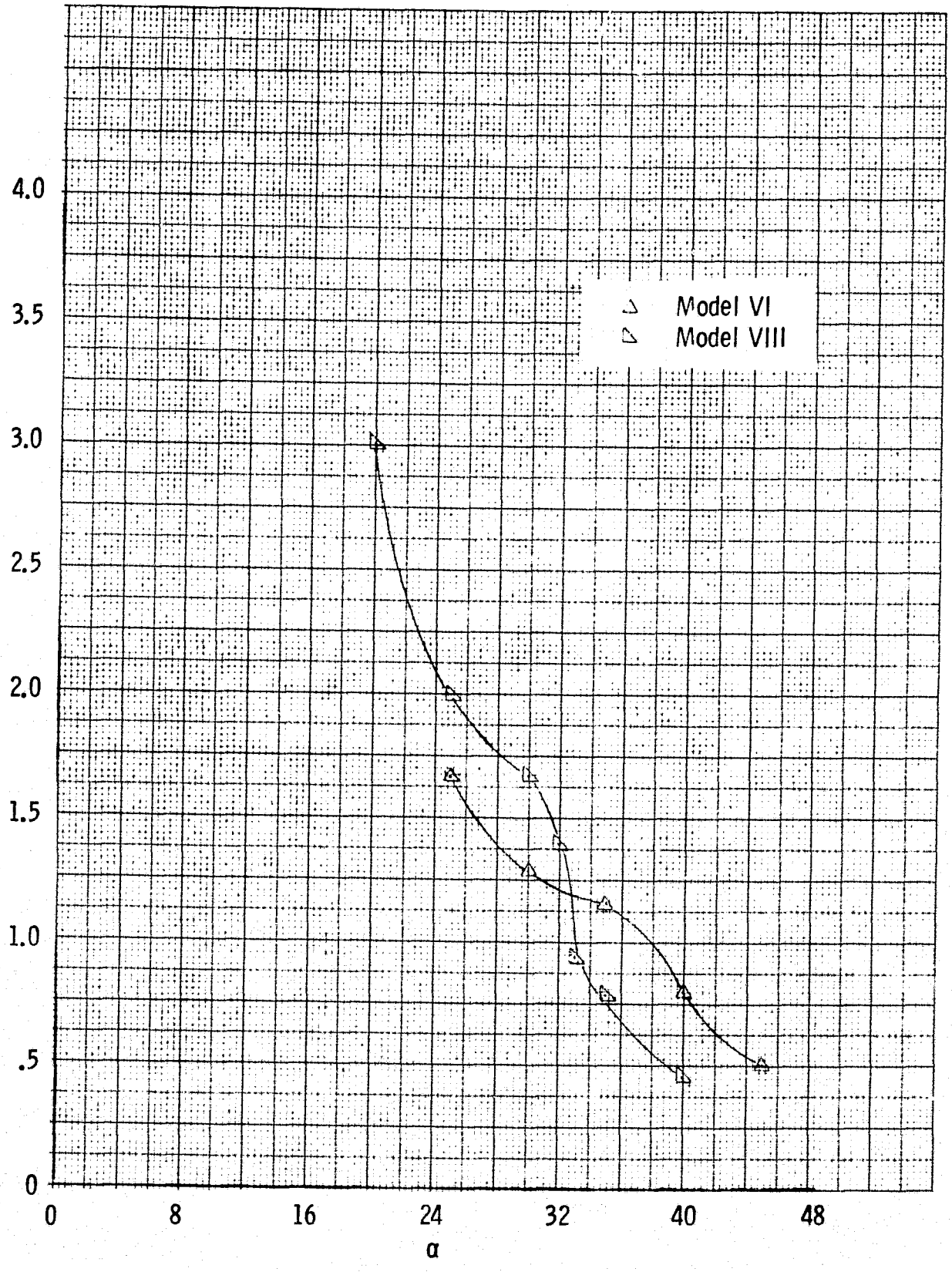

Figure 50. Vortex bursting position - Models VI and VIII.